



Organic persistent luminescence imaging for biomedical applications

Zelin Wu, Adam C. Midgley^{*}, Deling Kong^{**}, Dan Ding

State Key Laboratory of Medicinal Chemical Biology, Key Laboratory of Bioactive Materials for the Ministry of Education, College of Life Sciences, Nankai University, Tianjin, 700031, China



ARTICLE INFO

Keywords:

Organic persistent luminescence
Bioimaging
Biomedical application
Molecular probe

ABSTRACT

Persistent luminescence is a unique visual phenomenon that occurs after cessation of excitation light irradiation or following oxidation of luminescent molecules. The energy stored within the molecule is released in a delayed manner, resulting in luminescence that can be maintained for seconds, minutes, hours, or even days. Organic persistent luminescence materials (OPLMs) are highly robust and their facile modification and assembly into biocompatible nanostructures makes them attractive tools for *in vivo* bioimaging, whilst offering an alternative to conventional fluorescence imaging materials for biomedical applications. In this review, we give attention to the existing limitations of each class of OPLM-based molecular bioimaging probes based on their luminescence mechanisms, and how recent research progress has driven efforts to circumvent their shortcomings. We discuss the multifunctionality-focused design strategies, and the broad biological application prospects of these molecular probes. Furthermore, we provide insights into the next generation of OPLMs being developed for bioimaging techniques.

1. Introduction

Optical imaging methodology are important technical means of visualizing biological events in biomedical research, allowing rapid spatial resolution with high sensitivity [1–6]. The signal-to-background ratio (SBR) and sensitivity during traditional fluorescence imaging are impacted by real-time photobleaching and autofluorescence induced by the excitation light. Persistent luminescence imaging circumvents photobleaching whilst maintaining high sensitivity due to the elimination of the need for constant excitation light, which also aids in reduction of background noise from autofluorescence of biological tissues. Thus, persistent luminescence imaging enables deep tissue imaging with favorable signal-to-noise ratios and broader application prospects for *in vivo* optical imaging with high SBR and specificity [7–9].

Persistent luminescence is a unique optical process arising from reactive oxygen and nitrogen species (RONS) triggered luminescence (i.e., chemiluminescence) or delayed continuous photon emission over time following cessation of the excitation light (i.e., afterglow and phosphorescence) [10–13]. At present, persistent luminescence materials (PLMs) have been divided into inorganic or organic classifications. Inorganic PLMs (IPLMs) are composed of toxic heavy rare earth metals, which are accompanied by difficulties in surface modification, poor

biocompatibility, accumulation in tissues, and poor elimination from the body [14,15]. When IPLM imaging probes are used for diagnosis, they typically require to be in a pre-irradiated state before administration, which can be achieved with ultraviolet light exposure. Currently, the use of IPLMs remains limited for long-term monitoring or tracking *in vivo*, due to the short luminescence lifetime of IPLM imaging probes [16].

Organic PLMs (OPLMs) have the inherent advantage of being highly robust for long-lived emission, which makes it possible to capture images with temporal resolution long after excitation. Thus, in combination with modification and assembly that favors biocompatibility, OPLMs offer new strategies and wider adoption for *in vivo* bioimaging [17]. The excitation and emission spectra of OPLMs can be tuned by engineering the structure to meet the requirements of the intended application [18, 19]. Moreover, OPLMs with near-infrared (NIR) emission can facilitate deep tissue detection and light reactivation, which can circumvent restrictions associated with PLM imaging probe lifetime in long-term biological imaging applications. Many organisms and their tissues will emit autofluorescence under visible light excitation, which hinders detection and imaging using fluorescent probes. For example, the fluorescence wavelength range of serum protein in plasma is 325–350 nm, and the fluorescence wavelength range of NADP and bilirubin is 430–470 nm. Therefore, the sensitivity and accuracy of fluorescence analysis within

^{*} Corresponding author.

^{**} Corresponding author.

E-mail addresses: midgleyac@nankai.edu.cn (A.C. Midgley), kongdeling@nankai.edu.cn (D. Kong).

Table 1
Overview of organic persistent luminescence imaging.

Imaging modality	Molecular Sensors	SBR	Penetration depth	Lifetime	Detection sensitivity
Chemiluminescence	Luminol; <i>Cypridina</i> luciferin analogs; Dioxetanes; Peroxyoxalates	>1700	8 mm	Minutes ~ Hours	3-fold greater than fluorescence
Afterglow luminescence	Porphyrim derivatives; Semiconducting polymers	2922 ± 121	5 cm	Seconds ~ Hours	3-fold greater than fluorescence
Room-temperature phosphorescence	Organic dyes	~428	N/A	Microseconds ~ Minutes	Greater than fluorescence

the visible light spectra are directly affected. NIR emissions are outside of the visible spectra range, thus, NIR-I (emission peak, 800–1000 nm), and NIR-II (emission peak, 1000–1700 nm) probes avoid bioimaging interference from biological tissue autofluorescence [20,21]. Several reviews have been published on chemiluminescence, photoluminescence, and phosphorescence [22–26], yet there has been no unified standard for their classification in the context of OPLM imaging probes. This review aims to summarize recent developments across the three types of OPLMs for bioimaging, categorized based on their luminescence mechanisms: chemiluminescence, afterglow luminescence, and phosphorescence. These three types of OPLMs have their own characteristics in terms of penetration depth, fluorescence lifetime, and detection sensitivity (Table 1). Optimization of OPLMs is performed by screening for these aspects, such as assessment of penetration depth by signal detection through varying thicknesses of chicken tissues, assessment of lifetime by *in vivo* imaging system (IVIS) timelapse, and assessment of sensitivity and SBR is typically calculated from images captured using IVIS. In this review, we also provide examples of biomedical applications and discuss the current challenges and future directions for OPLMs.

2. Chemiluminescence imaging

Chemiluminescence (CL) is light produced following chemical reaction-induced molecular excitation [27]. Oxidation of the reactants results in the formation of oxidized high-energy intermediates that will either directly decay to ground state whilst emitting light or transfer their energy to nearby fluorophores, which in-turn produces luminescence. The commercial development of charge-coupled device (CCD) detectors with high sensitivity and resolution has resulted in the widespread

adoption of CL imaging techniques to detect various analytes in the field of biochemical analysis [28]. Due to the absence of external light excitation, CL avoids the issue of background autofluorescence that exists in traditional fluorescence techniques. Thus, CL can achieve high SBRs and sensitivity in biological imaging [29].

CL probes are implicated in the construction of CL-based imaging systems to replace traditional fluorescence imaging in the monitoring of reactive oxygen species (ROS) indicative of disease and tumor biomarkers. These include luminol and *Cypridina* luciferin analogs [30–32], which undergo oxidation reactions accompanied by CL emission [33,34]; and 1,2-dioxetane derivatives and peroxyoxalates, which react with ROS to produce CL products [35–37]. A growing number of new imaging and therapeutic applications are utilizing CL [38–41]. Therefore, a systematic generalization and timely survey of advances in the field of CL probes is a requirement. In this section, we summarize four type of CL probes and give examples of their biological applications.

2.1. Luminol and luminol analogs

Luminol CL was first reported by Albrecht in 1928, wherein horseradish peroxidase (HRP) was demonstrated to catalyze the oxidation of luminol by hydrogen peroxide (H_2O_2) [42]. Luminol and its analogs have been widely used in biosensing and bioimaging techniques due to their simplistic synthesis, water solubility, stable properties, and high CL efficiency [43–45]. In 2016, Park and colleagues combined poly(ethyl glycol) (PEG) with a luminol analog (L012) to develop NIR hybrid nanoparticles (HNPs) with peak emission at a wavelength of 780 nm [46]. L012 produced CL at approximately 460 nm in the presence of H_2O_2 , which overlapped with the excitation wavelength of PEG quantum

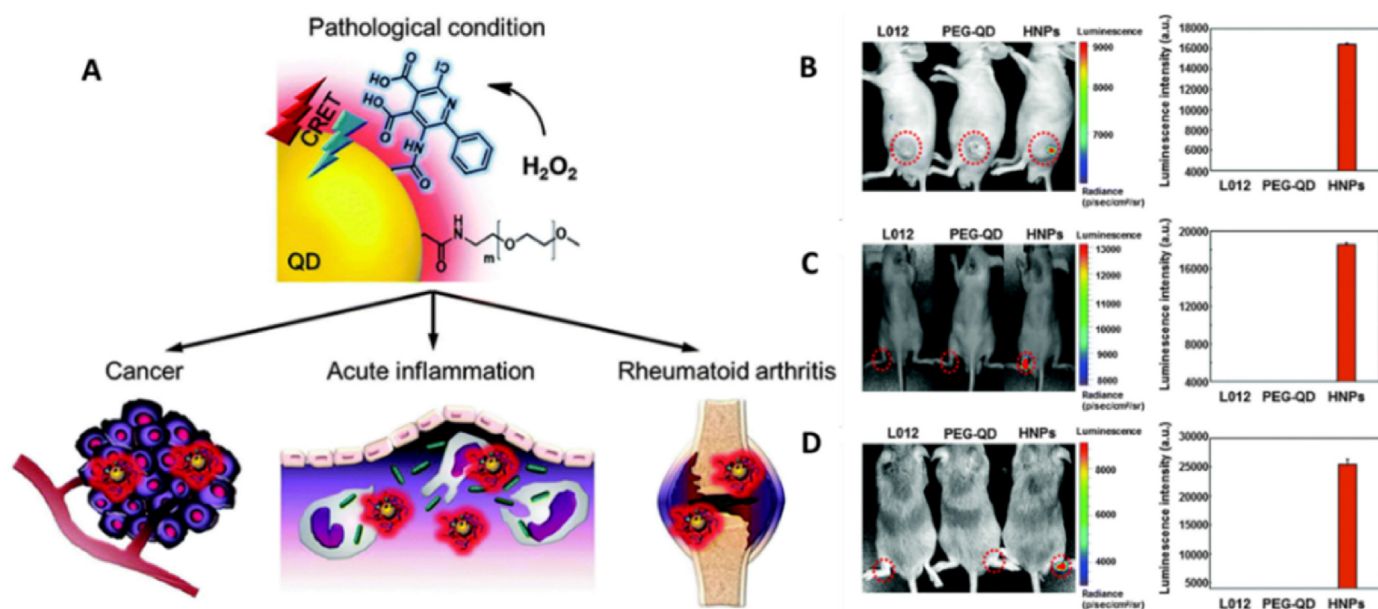


Fig. 1. (A) Schematic of HNP-based detection of H_2O_2 overproducing diseases. *In vivo* imaging of (B) PC3 cancer cell line induced tumor mouse models, (C) lipopolysaccharide induced inflammation mouse models, and (D) collagen-induced arthritis mouse models [46].

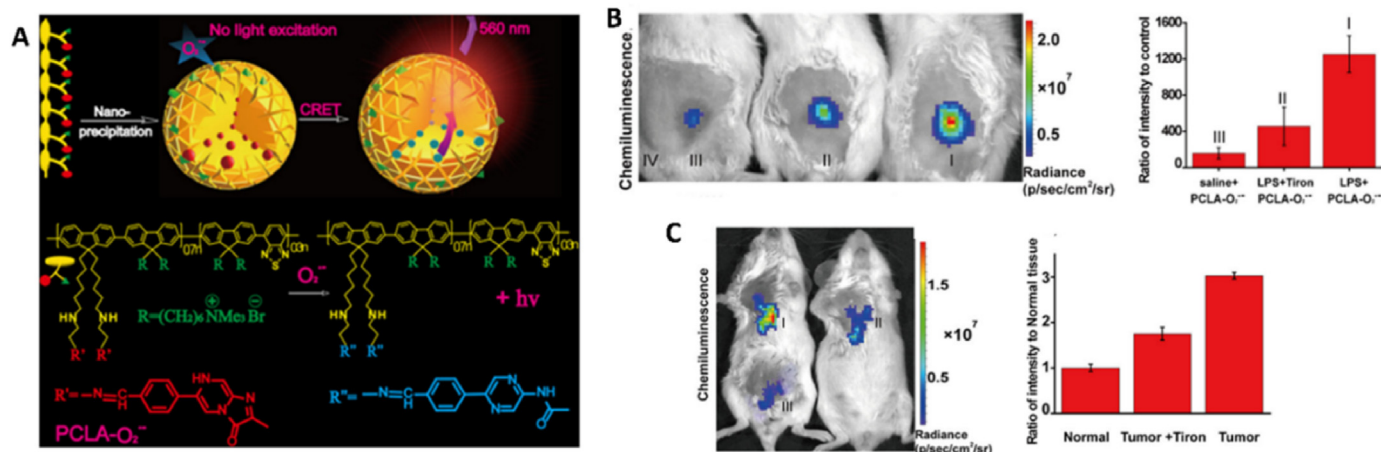


Fig. 2. (A) Schematic illustration of the CL nanoprobe preparation by nanoprecipitation and the final chemical structure of PCLA-O₂⁻. (B) CL imaging and quantification of emission intensities resulting from LPS induction of O₂⁻ production, in the presence or absence of the O₂⁻ scavenger Tiron. (C) CL imaging of ultra-low O₂⁻ concentrations in mouse tumor models [49].

dots (QDs), resulting in their NIR emission (Fig. 1A). The authors constructed three overproduction disease models associated with H₂O₂ overproduction, namely tumor (Fig. 1B), acute inflammation (Fig. 1C), and arthritis (Fig. 1D) models. The CL intensity of HNPs was high in all three models, which suggested that the authors' luminol-based CL imaging system has the potential to serve as a powerful and diagnostic tool for H₂O₂-related diseases.

2.2. Cypridina luciferin analogs

In 1957, Goto and colleagues isolated and crystallized *Cypridina* luciferin from the sea firefly, *Cypridina hilgendorffii* [47]. Following its oxidation in the presence of luciferase enzyme, *Cypridina* luciferin emits a blue CL light, and can be achieved at neutral pH. Thus, *Cypridina* luciferin analogs with imidazopyrazinone structures have been developed as novel

and specialized detection systems for the presence of superoxide (O₂⁻) in biological applications [48]. Tang et al. reported a CL resonance energy transfer (CRET)-based polymer nanoprobe (PCLA-O₂⁻) for the *in vivo* imaging of native O₂⁻ presence to differentiate tumor tissues from healthy tissues [49]. The system used imidazopyrazinone-type luciferin moieties (CHO-CLA) that served as both recognition units for O₂⁻ and as energy donors. The quaternary ammonium group-containing conjugated polymer, PFBT, was both the energy receptor and a signal amplifying substrate, while providing a hydrophobic environment to enhance prolonged CL intensity (Fig. 2A). The results showed that the CL half-life of this system was significantly longer than that of CHO-CLA alone, and its detection limit was 19.3 pM. The CRET-nanoprobe system successfully achieved highly sensitive imaging of intrinsic ultra-low O₂⁻ concentrations in lipopolysaccharide (LPS)-induced inflammation (Fig. 2B) tumor-bearing mice (Fig. 2C).

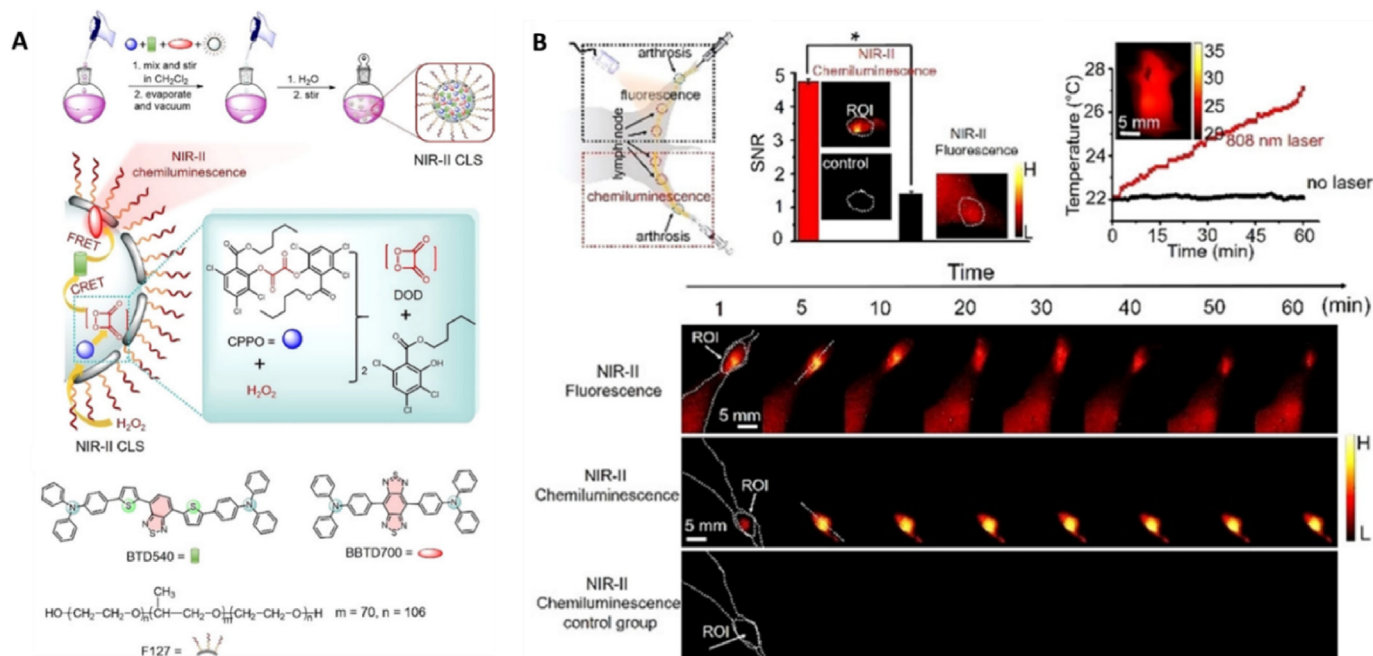


Fig. 3. (A) Schematic illustration of the preparation method for NIR-II CLS, which emit CL light in the presence of H₂O₂. (B) Results of NIR-II CLS versus fluorescence detection of inflammatory neutrophil imaging in lymph nodes and arthritis models [64].

2.3. Dioxetanes

In 1982, Schaap's group discovered a unique chemical excitation pathway that occurred in the molecules containing the specific structure of 1,2-dioxetane with a protected phenolic substituent in the para position [50]. Dioxetanes and their derivatives are promising adaptable CL tools for detecting various biological analytes [51–57]. However, CL selectively triggered by enzymatic or analyte-dependent reactions tend to exhibit low CL efficiency, representing a key limitation of their application. Recently, work by Shabat et al. presented a solution for low-efficiency light emission [58]. The team developed a highly selective and sensitive probe, named HOCl-Cl-510, which detected HOCl *in vitro* and *in vivo*. Through tuning of the specific HOCl-sensing moiety, stable HOCl intermediates and bright CL detection in real-time was achieved in acute and chronic inflammation models. This work successfully provided a new CL tool for dynamic monitoring of disease development [59].

2.4. Peroxyoxalates

Peroxyoxalate CL (POCL) has the advantages of being highly sensitive to H_2O_2 microenvironments and has long-lasting activity [60–63]. POCL is based on the non-radioactive dipole-dipole energy transfer processes resulting from the chemical reaction of H_2O_2 with peroxyoxalic acid. The high energy intermediate 1,2-dioxanedione intermediate (DOD) is formed and transfers its energy to a suitable coexisting fluorophore acceptor, resulting in its excitation and emission of light upon returning to ground state. A major disadvantage of peroxyoxalates is their poor solubility. To prevent the spontaneous hydrolysis of peroxyoxalates in aqueous media and enable its better applicability *in vivo*, most peroxyoxalate and dyes are co-encapsulated in stable micelles or nanoparticles to enhance water solubility and achieve efficient chemical energy transfer in response to tissue microenvironments.

In 2020, Yang et al. reported a second near-infrared (NIR-II) CL sensor (NIR-II CLS) that achieved high-contrast *in vivo* imaging of inflammation

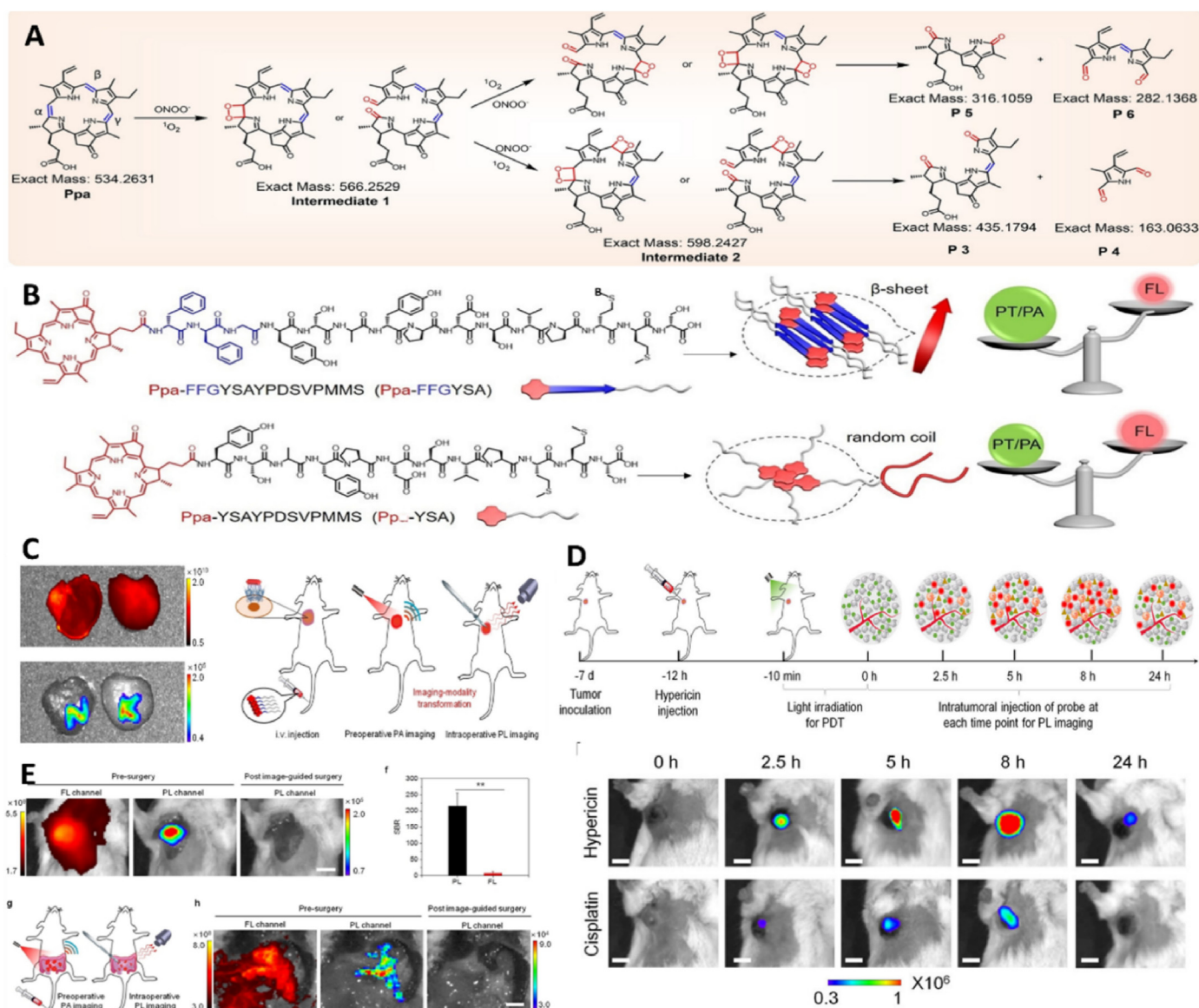


Fig. 4. (A) Chemical schematic of Ppa formation. (B) Chemical structures of Ppa-FFGYSA and Ppa-YSA that self-assemble to form supramolecular β -sheets and random coil nanomodules, respectively. (C) Fluorescence (FL) and persistent luminescence (PL) in isolated livers. (D) Schematic explanation of reactivated persistent luminescence of Ppa-FFGYSA and intratumoural injection. (E) Representative FL and PL images of guided orthotopic breast tumor resection before and after surgery [71].

imaging based on a classical POCL system [64]. The team used two donor-acceptor-donor fluorochromes, BTD540 and BBTD700 which converted the CL donor (DOD) to emit high-energy NIR-II photons by integrating sequential CRET and fluorescence resonance energy transfer (FRET) processes. The large Stokes shift of the two fluorochromes together with the high FRET efficiency between them dictated the achievement of highly efficient NIR-II CLS (Fig. 3A). Furthermore, H_2O_2 selectively activated NIR-II CLS, facilitating the *in vivo* detection of H_2O_2 -induced local inflammation in lymphatic and joint regions of mouse models over a prolonged period whilst exhibiting deep tissue penetration (Fig. 3B). When compared with NIR-II fluorescence sensors

employed in the same models, NIR-II CLS demonstrated a 4.5-fold improvement in SBR, indicative of the potential for NIR-CL systems for *in vivo* biosensing.

Yu et al. constructed anti-tumor drug (lapachone)-loaded H_2O_2 -responsive CL nanoparticles (L-HPOX) for precision imaging and treatment of tumors. Pluronic F-127 (PF127) and oxalate containing polymer (POE) were assembled into lapachone-loaded nanoparticles by hydrophilic and hydrophobic methods [65]. Co-delivery with H_2O_2 or LPS demonstrated the localized CL emission by L-HPOX was achieved and could be detected *in vivo*. The tumor content of H_2O_2 increased after treatment by 5,6-dimethylxanthone-4-acetic acid and L-HPOX could then

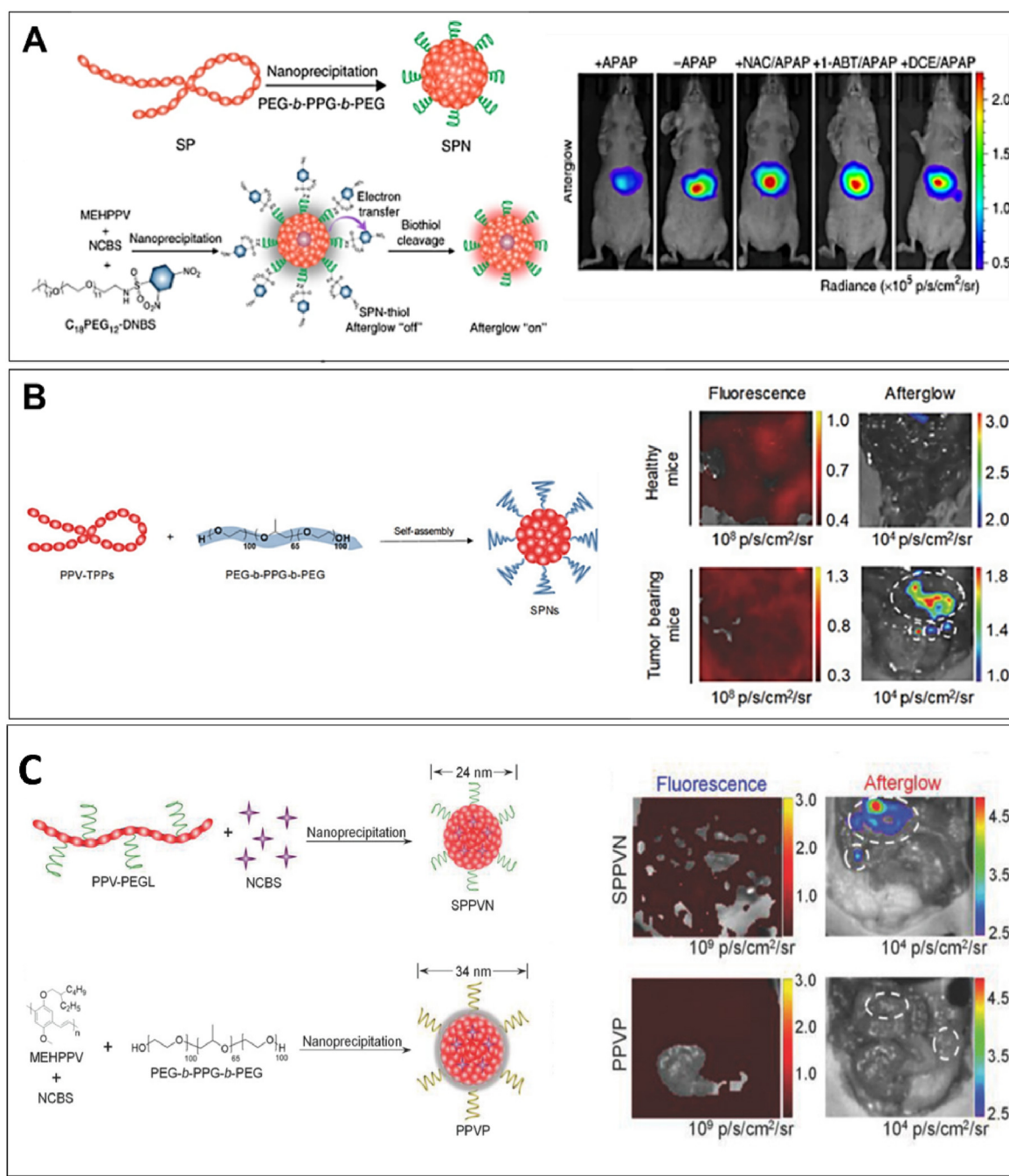


Fig. 5. (A) Synthesis of SPNs and biothiol-activated SPNs with AL imaging in drug-challenged hepatotoxicity mouse models [75]. (B) Synthesis of PPV-TTP SPNs and fluorescence versus AL imaging in peritoneal metastatic tumors, 4 h after injection of SPN2.5 [76]. (C) Synthetic routes of SPPVN and PPVP and fluorescence versus AL imaging in peritoneal metastatic tumors, 1.5 h after injection of SPPVN [77].

track tumors *in vivo* via H₂O₂ induction of CL. The CL imaging by L-HPOX resulted in higher SBR over 12 h and provided a more accurate diagnostic indication of tumor presence and location *in vivo*.

The above works demonstrated that compared with traditional fluorescence imaging, CL imaging has removed the requirement for excitation light, thereby lowering background noise and enhancing sensitivity and SBR. Taken together with the flexibility in molecular design that can be tuned according to the application needs, the advantages described across these exemplar studies indicate that CL imaging probes have promising biological application prospects.

3. Afterglow luminescence

Afterglow luminescence (AL) imaging is a new optical imaging

paradigm that can be employed to detect the spontaneous emission by specific organic analytes after photoexcitation has stopped [66–69]. Under laser irradiation, photosensitive poly(p-phenylenevinylene) (PPV) semiconductor polymers become photosensitized, and the vinyl bonds of the semiconductor backbone react with ¹O₂, which forms high-energy dioxane intermediates via $\pi^2-\pi^2$ cycloaddition reaction [70]. These intermediates undergo delayed spontaneous decomposition while emitting AL light. Compared with traditional fluorescence imaging, surplus AL imaging has the merits of low background noise, high sensitivity, and considerable tissue penetration depth. The long-lasting emissions have clinical potential as AL is not subject to spontaneous fluorescence interference from tissue autofluorescence.

Typically, porphyrins are used as photothermal agents, photosensitizers, and fluorescence agents. Recent work from the Ding lab reported

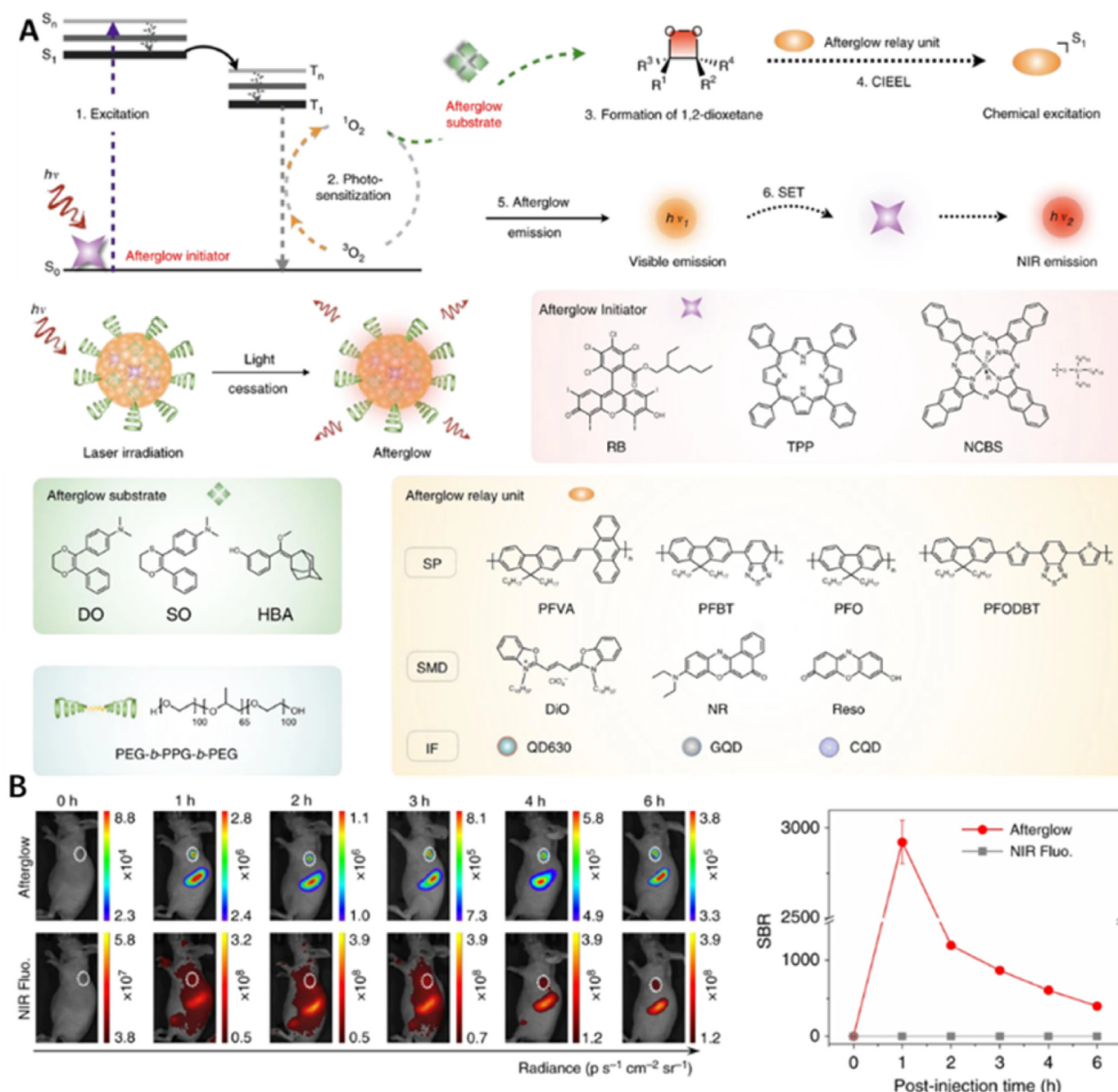


Fig. 6. (A) The mechanisms of AL and design of ALNPs consisting of AL initiator, substrate, and relay unit. (B) Representative ALNPs demonstrating AL and AL and NIR fluorescence imaging at the different time points in 4T1 tumor-bearing mice [78].

the novel finding that porphyrins exhibited intrinsic NIR persistent luminescence and AL, in the presence of peroxyinitrite (ONOO^-) during and after exposure to photoexcitation [71]. The authors screened several persistent luminescence properties of porphyrin derivatives (Fig. 4A) and found that pyropheophorbide A (Ppa) had higher sensitivity to ONOO^- and generated bright persistent luminescence signals that peaked at 760 nm over a duration of 60 min. The authors then modified Ppa with peptides containing self-assembly units (Ppa-FFGYSA) to attain supra-molecular self-assembling and active tumor targeting nanomodules (Fig. 4B). The nanomodules possessed enhanced photoacoustic and continuous AL signals, as evidenced by real-time imaging in liver tissue (Fig. 4C). The data suggested that Ppa nanomodules were conducive to preoperative photoacoustic localization and intraoperative continuous AL imaging of tumors to guide resection (Fig. 4D). Light-triggered functional conversion from photoacoustic imaging to continuous AL imaging was achieved in two tumor models of murine breast cancer and peritoneal cancer *in situ* (Fig. 4E). As a marker of neutrophil infiltration and immunogenic cell death, ONOO^- detection by Ppa-FFGYSA nanomodules holds promise for clinical translational prospects of AL-assisted imaging.

The ultra-sensitive prospects of AL for *in vivo* imaging are limited by its dependence on inorganic carrier nanoparticles with difficult to modify surfaces, which may contribute to short NIR emission lifespan and relative dampening of signal contrast in target tissues [72–74]. A series of works by the Pu lab sought to address these issues using organic AL nanoconstructs. In 2017, the group fabricated organic <40 nm optically active semiconducting polymer nanoparticles (SPNs) that demonstrated emission detection peaks at 780 nm that penetrated through living mouse tissue and had an emission half-life of about 6–7 min [75]. Dioxetane formation was intrinsically determined by substituent groups of the phenylenevinylene (PPV) polymer's vinyl bonds, and the PPV-SPNs could generate the necessary reactive $^1\text{O}^2$ for AL emission following light irradiation. Incorporation of NIR-absorbing $^1\text{O}^2$ sensitizer, NCBS5, facilitated recharged AL in deep tissue for longitudinal *in vivo* imaging. Thus, SPN-NCBS5 permitted rapid and highly sensitive lymph node and tumor imaging. Furthermore, by taking advantage of the structural versatility of SPNs, the authors developed smart biorthiol-activatable

NIR-AL probes (SPN-thiol) that could be activated by endogenous anti-oxidant biorthiols present shortly after drug challenge in drug-induced hepatotoxicity. The SPN-thiols produced a SBR level that was 25-fold greater than NIR fluorescence (Fig. 5A).

In their 2018 investigation, the same team designed and synthesized PPV-SPNs that containing co-polymerized tetraphenylporphyrin (TPP), a NIR photosensitizer, for *in vivo* AL imaging of tumors in mice [76]. Based on AL intensity determination by the amount of high-energy PPV-dioxetane generated, PPV-SPNs were designed to exploit FRET and TPP promotion of $^1\text{O}^2$ generation, thereby amplifying AL. The constructed SPNs (SPN2.5) showed the NIR AL peaks at 720 nm with an intensity 6.12-fold brighter than the nanoparticles without TPP (SPN0). The oxygen-sensitive AL of SPN2.5 was useful for *in vivo* imaging of tumor hypoxia and tiny peritoneal metastatic tumor tissues in living mice could be detected following systemic administration of SPN2.5, a feat that could not be replicated by fluorescence imaging alone (Fig. 5B). In the same year, the Pu lab reported their advancements in ultrasensitive imaging of living mouse metastatic tumors using amphiphilic polystyrene derivatives self-assembled into nano agents (SPPVN) that emitted NIR AL [77]. Doping of PPV-PEG nanoparticles with 2% NCBS photosensitizer, facilitated improved FRET efficiency, the generation of $^1\text{O}^2$ by light irradiation, and enhanced AL intensity at a peak emission of 780 nm and 20-fold greater brightness than PPV-PEG nanoparticles without NCBS. The SPPVN nanoparticles emitted a bright and persistent NIR AL that penetrated deep tissue to a depth of up to 1.6 cm, facilitating peritoneal metastatic tumor detection and outperforming fluorescence imaging, with SBRs of 602 ± 104 and 40 ± 3 , respectively (Fig. 5C). In addition, SPPVNs were highly sensitive to oxygen levels and accumulated in tumors. The resulting AL enabled real-time live imaging of oxygen levels in the mouse tumors as small as 1 mm^3 and in microscopic peritoneal metastases.

In 2019, the Pu group reported on transforming fluorescent agents into AL nanoparticles (ALNPs) for *in vivo* imaging [78]. Their approach relied on an intraparticle cascade photoreaction of three components: the AL initiator (photosensitizer to generate $^1\text{O}^2$), substrate ($^1\text{O}^2$ -reactive molecule to promote unstable 1,2-dioxetane formation), and a relay unit (fluorescent agent to accept energy transfer from 1,2-dioxetane and

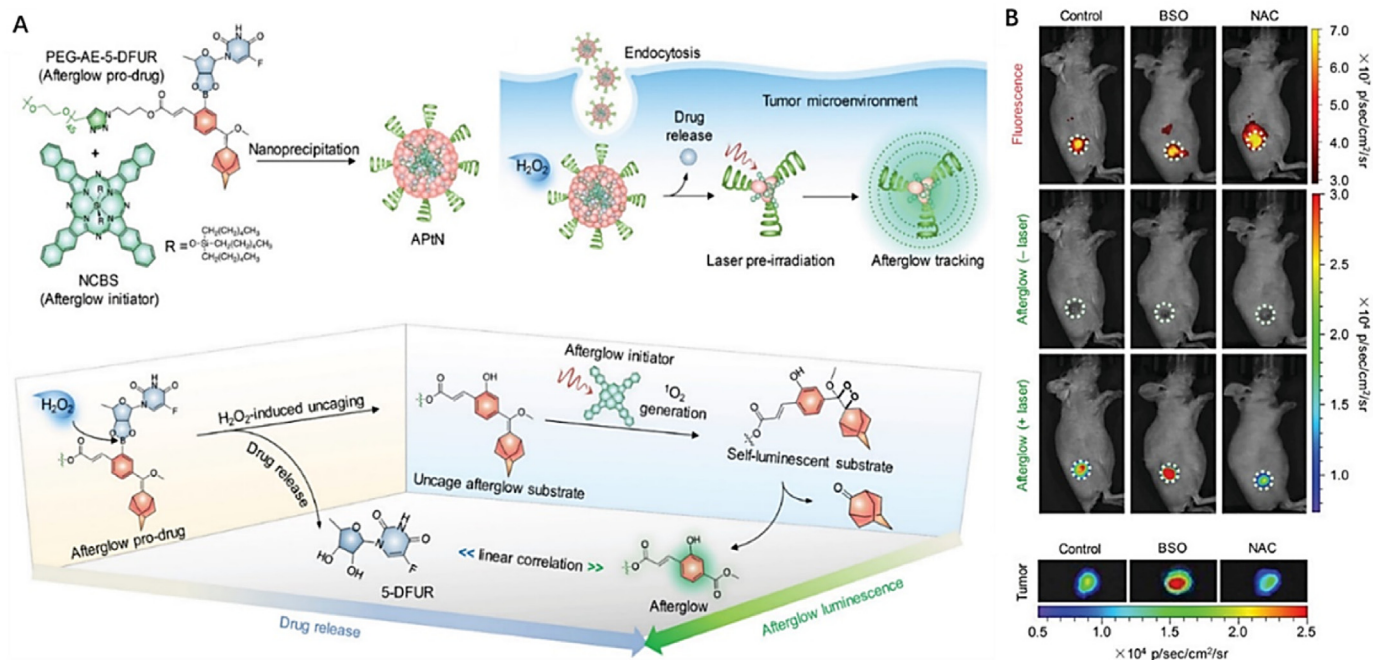


Fig. 7. (A) Design and proposed mechanism of APTn for cancer theranostics. (B) NIR fluorescence imaging and comparisons to AL imaging of 4T1 tumor-bearing mice, imaged 24 h after intravenous injection of APTn [79].

gradually release it in the form of photons). Together, these components enable the storage of photoenergy as chemical defects for delayed AL after cessation of photoexcitation (Fig. 6A). The team demonstrated that different combinations of material components resulted in discrepancies in fluorescence and AL spectral profiles. This was suggested to be ascribed to the AL photophysical process differing from the fluorescence process. In fluorescence processes, light excitation leads to direct emission by the fluorescent agent, which is followed by potential energy transfer to the photosensitizer; whereas, in AL processes, in addition to potential energy transfer, photosensitizers are directly excited by the energy released from high-energy intermediates (e.g., 1,2-dioxetane). Thus, the authors concluded that photophysical interplay between the AL initiator and relay unit offers the capability to fine-tune ALNPs to potentially enable multiplexed imaging. Using ALNPs comprised of poly

[(9,9'-dioctyl-2,7-divinylene-fluorenylene)-alt-(9,10-anthracene)], NCBS, and *N,N*-dimethyl-4-(3-phenyl-5,6-dihydro-1,4-dioxin-2-yl) aniline (PFVA-N-DO) as an example, the AL achieved a maximal imaging depth at 5 cm in biological tissue, deeper than other reported AL agents (4 cm). As compared with NIR fluorescence, the AL exhibited three orders of magnitude higher SBR (2922 ± 121), allowing for faster detection of tumors in living mice after systematic administration (Fig. 6B). This was the highest SBR achieved thus far for *in vivo* optical imaging, regardless of optical modalities and detection wavelengths. In addition, the representative PFVA-N-DO ALNPs were enzymatically biodegradable and clearable, demonstrated long-term biocompatibility. Such a controllable nanoengineering approach has potential applicability to multiple fluorophores, regardless of their composition, for reduced background optical imaging techniques.

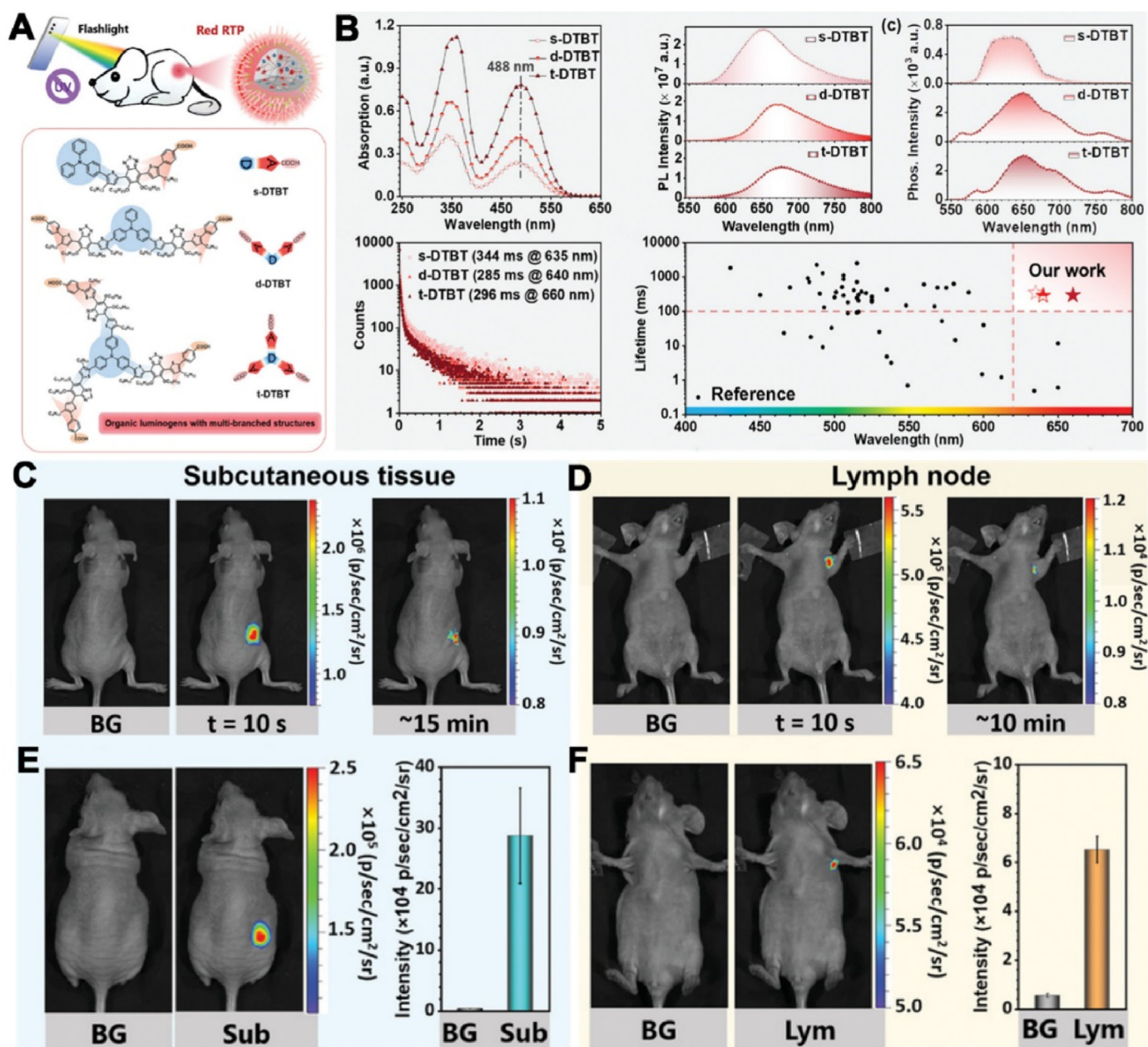


Fig. 8. (A) Schematic illustration of red RTP excitation by mobile phone flashlight and chemical structures of the DTBT linear and branched derivatives. (B) Photophysical properties of luminogens s-DTBT, d-DTBT, and t-DTBT. Sunlight excitation of RTP bioimaging in the (C) subcutaneous tissue and (D) lymph nodes of mice. Mobile phone flashlight excitation of RTP bioimaging in (E) subcutaneous tissue and (F) lymph nodes of mice [100]. (For interpretation of the references to colour in this figure legend, the reader is referred to the Web version of this article.)

In their follow-up study, Pu et al. presented a novel excitation-free and smart cancer theranostic nanoagent that enabled tumor-activated drug release with signal correlation that used their previously established three-factor ALNP design. The team reported the synthesis of an organic amphiphilic AL nanoassemblies with protheranostic functions (APtN) to elicit pharmaceutical effects and diagnostic signals in tumor microenvironments (Fig. 7A) [79]. APtNs were self-assembled from hydrophilic PEG, conjugated via a H_2O_2 -sensitive linker to hydrophobic AL substrate adamantylidene-enol ether (AE) and antitumor prodrug 5'-deoxy-5-fluorouridine (5-DFUR), and co-assembled with AL initiator NCBS. APtNs passively targeted tumors after systemic injection by exploiting the enhanced permeability and retention (EPR) effect. Following their accumulation in the H_2O_2 -enriched tumor microenvironment, APtNs were cleaved to release 5-DFUR and PEG-AE. Subsequent NIR laser irradiation of NCBS initiated 1O_2 generation, which in-turn reacted with the uncaged AE and led to the formation of high-energy PEG-dioxetane intermediates. Such an organic nanoassembly addressed the need for a theranostic response as triggered by the tumor microenvironment. The AL of APtN was enhanced 820-fold in solution after H_2O_2 addition, and the signal intensity correlated with released amount of the 5-DFUR. The *in vivo* results recapitulated the AL signal enhancement in elevated ROS tumor microenvironments, providing superior real-time imaging of tumor location (Fig. 7B) and prodrug activation status.

4. Room-temperature phosphorescence imaging

Phosphorescence imaging is an emerging photoluminescence imaging method that does not rely on external real-time photoexcitation and is undisturbed by tissue autofluorescence. Phosphorescence imaging

belongs to the afterglow luminescence classification, but the mechanisms of luminescence and reactivation are different. Phosphorescence techniques can provide high-quality and high-resolution imaging with higher SBRs [80–82]. Long-lived room-temperature phosphorescence (RTP) materials have considerable application and translational potential in clinical bioimaging, organic electroluminescent diode (OLED) manufacture, advanced anti-counterfeiting techniques, and biochemical sensors design [83–85]. The majority of developed long-lasting RTP materials have been organometallic complexes or inorganic compounds, which have the associated disadvantages of poor stability, high production cost, elevated risk of toxicity, and difficulty for aqueous modification, deeming them unsuitable for biomedical imaging applications [86–88]. Therefore, a research hotspot has become evident in recent years – the development of organic long-lived RTP materials with green manufacture, facile modification, high stability, and good biocompatibility at a reduced production cost. However, few studies on organic RTP materials for bioimaging have been reported [89].

To meet requirements for *in vivo* bioimaging, three key factors are necessary to include in organic RTP design, the ability to: (i) promote intersystem crossing (ISC); (ii) stabilize fragile triplet excitons; and (iii) suppress non-radiative decay [90]. Two methods to achieve this are based on first-order perturbation theory and the Marcus semi-classical method. The first introduces spin-orbit coupling (SOC) with lone pairs of electrons. Heavy atoms, carbonyl groups, and heteroatoms (N, P, etc.) can enhance SOC [91,92]. The second method stabilizes fragile triplet excitons in rigid environments by suppressing non-radiative relaxation pathways through crystal formation, supramolecular assembly, H-aggregation, and host-guest doping [93,94]. Additionally, good water dispersibility and stability are requirements for biomedical applications [95]. In this regard, special attention should be paid to protecting fragile

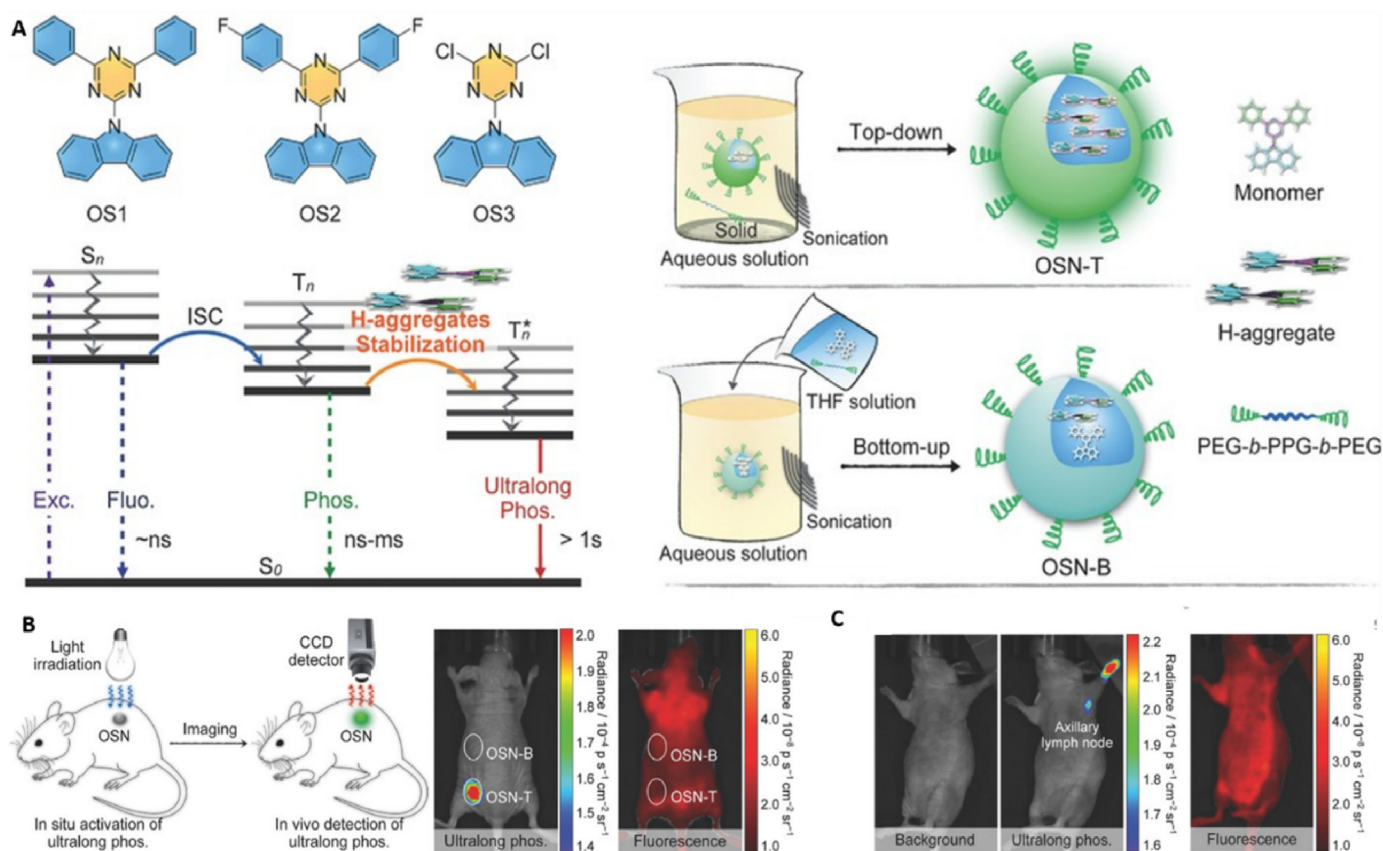


Fig. 9. (A) Chemical structures of organic semiconductors utilized, and schematic illustration of the differential preparation methods for OSNs-T and OSNs-B. (B) Schematic illustration and ultralong RTP and fluorescence imaging of a mice injected with the subcutaneous inclusions of OSNs. (C) Ultralong phosphorescence and fluorescence imaging of lymph node in living mice [101].

triplet excitons from quenching effects of oxygen and water [96]. At present, the phenomenon of long-lived RTP is predominantly represented by crystal structures, which restricts design to nanocrystalline structures to improve administration routes and biocompatibility [97,98]. In the following section, we focus on the current progress of breakthroughs in the RTP materials field for biological applications.

4.1. Engineering enhanced performance organic persistent RTP luminogens

Wang et al. employed a class of amide derivatives with high RTP efficiency by introducing spin-orbit coupling-promoting groups to the π -unit and aromatic-unit, obtaining robust persistent RTP (p-RTP) luminogens [89]. The various developed p-RTP luminogens demonstrated impressive efficiency and lifespan, as high as 10.2% and 710.6 ms, respectively. Two of the luminogens exhibited strong RTP after mechanical stimulation, which was indicative of their strengthened stability. Furthermore, whilst in an amorphous state, the p-RTP luminogens showed evident potential for bioimaging. Phosphorescence imaging in live mice showed that the highly robust p-RTP luminogens had exceptionally high SBR of 428, demonstrating the feasibility to obtain potent and robust RTP despite being derivative from unprotected organic materials.

In 2019, Yuan et al. synthesized a series of highly efficient pure organic p-RTP based on carbazole and benzoic acid moieties [99]. The team eliminated the larger methyl group, which contributed to the denser molecular packing present in the crystal structure. Efficient hydrogen bonding from the presence of more carboxyl groups produced highly rigid conformations that ultimately benefited the lifetime and efficiency of p-RTP, attributed to stabilized triplet excitons. Water-dispersed nanoparticles were prepared from the p-RTP compounds and achieved phosphorescence emission SBR as high as 62 when used for *in vivo* bioimaging. These results suggested that molecular and crystallographic precision engineering can have broad application prospects for high-performance pure organic p-RTP emitters.

RTP luminogens typically emit green or yellow light with shallow tissue penetration whilst requiring excitation by potentially hazardous ultraviolet (UV) lamps, thus limiting their applicability in clinical bioimaging. A recent study by Fan et al. demonstrated that the rational combination of an electron donor (D) and acceptor (A) with different structural geometries and numbers, facilitated strong intramolecular charge transfer through D- π -A systems with linear and branched structures (Fig. 8A) [100]. The organic benzothiadiazole-based (DTBT) RTP luminogens had increased molar extinction coefficients, which benefited

efficient light harvesting and excitation, and emitted long-wavelength (red) light with improved tissue penetration depth. Moreover, the red RTP were photo-excitabile by visible light from a mobile phone flashlight. The red RTP emitted light at approximately 650 nm and exhibited a phosphorescence life span for as long as 344 ms, which is currently the longest lasting example of a pure organic red RTP material (Fig. 8B). Due to the absorption of visible light and the continuous RTP emission by single-branched structure DTBT (s-DTBT) nanoparticles, the p-RTP imaging in the subcutaneous tissue (Fig. 8C) and lymph nodes (Fig. 8D) lasted for 10 min, indicative of their use for real-time detection. Even with a low-powered flashlight, p-RTP imaging following systemic injection achieved a high SBR of 230 in subcutaneous tissue (Fig. 8E) and lymph nodes (Fig. 8F). This study provided a route towards safe bioimaging methods that are accessible in any clinical setting. At present, organic p-RTP probes are still in their infancy in the context of biomedical applications. Due to their advantages of high sensitivity, high SBR, and biocompatibility, organic p-RTP probes represent a field with high development potential for a broad range of bioimaging applications.

4.2. Top-down synthesis of RTP nanoparticles for bioimaging

In 2017, the Pu group prepared a series of organic semiconductor nanoparticles (OSNs) using PEG-*b*-PPG-*b*-PEG as a matrix to stabilize the nanocrystals and protect them against oxygen quenching [101]. They used a top-down approach to prepare nanoparticles (OSNs-T; 70–80 nm) from solid crystals of organic phosphorescent semiconducting dyes, whilst bottom-up nanoprecipitation was used to synthesize nanoparticles (OSNs-B; 20 nm) from homogeneously dissolved tetrahydrofuran (THF) solution of the crystal dyes (Fig. 9A). Both OSNs showed appropriate cytocompatibility and water solubility, but OSNs-T had a wider adsorption range than OSNs-B, which indicated that its H-aggregates had stronger molecular packing. H-aggregation favors stabilization of triplet excitons; thus OSNs-T showed a longer lifetime and higher RTP intensity than OSNs-B (0.861 s versus 0.492 s). Following removal of external light source, *in vivo* imaging results indicated that subcutaneous OSNs-T brightness was approximately 22-fold greater than OSNs-B (Fig. 9B), which supported the indispensability of top-down synthesis methods to stabilize triplet excitons. Given the lack of autofluorescence, visualization of lymph nodes was clear (SBR \approx 40), whereas fluorescence emission made it difficult to determine the location of the lymph nodes (Fig. 9C).

In 2018, Li and Pu devised a series of 10-phenyl-10H-phenothiazine 5,5-dioxide derivatives (CS), as characterized by their different para substituents (Fig. 10A) [102]. The CS compounds showed adjacent

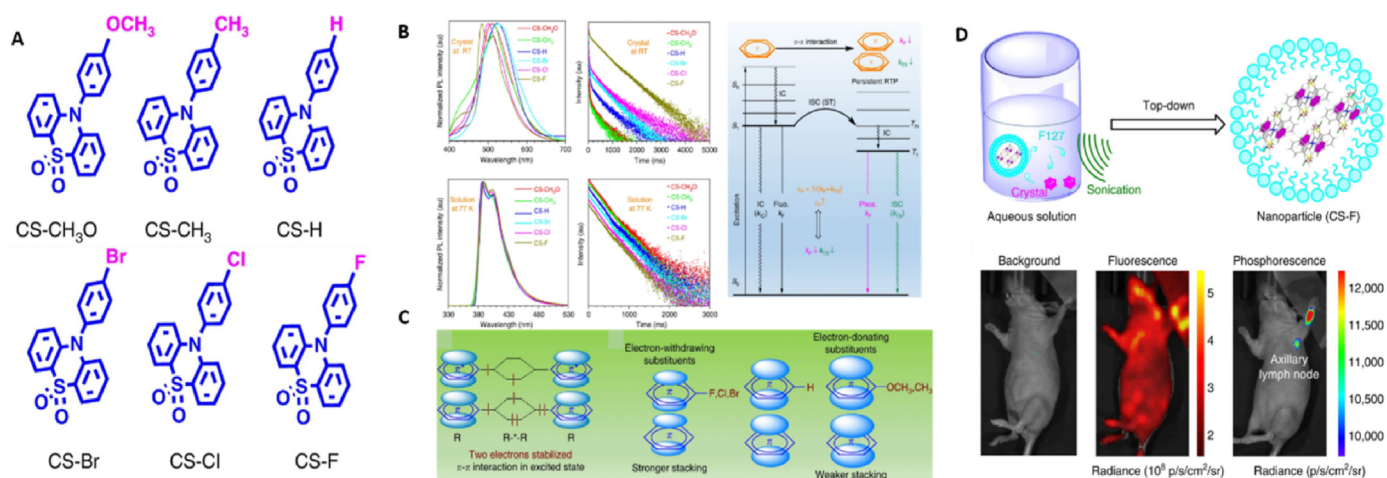


Fig. 10. (A) The molecular structures of the six CS RTP compounds. (B) The phosphorescence spectra and corresponding time-resolved decay curves for the six CS RTP compounds. (C) The influence of π - π interactions on the electron redistribution and RTP behavior. (D) *In vivo* real-time excitation-free phosphorescent imaging of lymph nodes following intracutaneous injection [102].

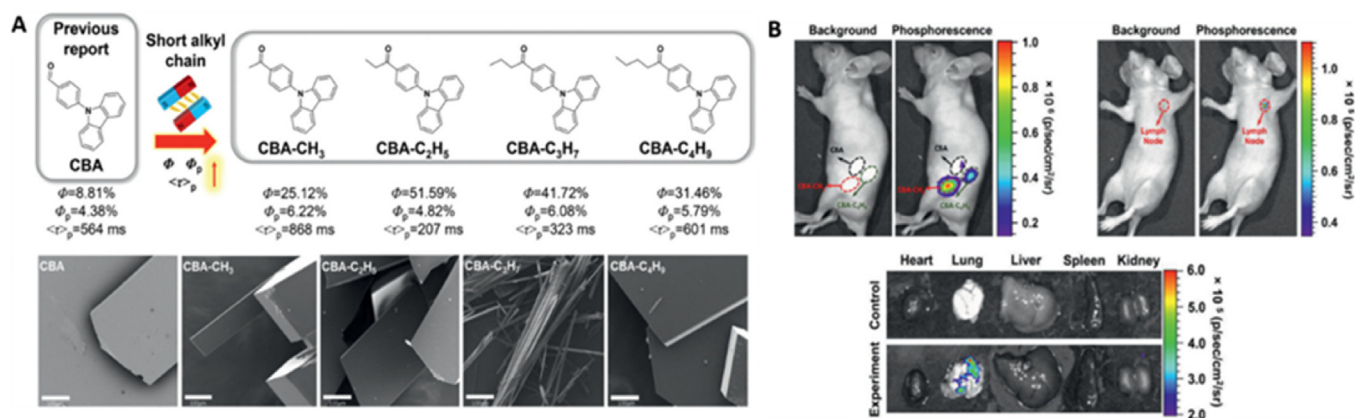


Fig. 11. (A) Chemical structures and corresponding scanning electron microscope (SEM) images of CBA crystals. (B) Time-resolved phosphorescence imaging of a mouse and lymph node and different organs [105].

phosphorescence emission bands with the approximate range of 500–600 nm. The CS-F showed a double emission peak due to its long lifetime and electron-withdrawing groups (Fig. 10B). The crystal structure changed from the original to phosphorescence state following irradiation with UV light for 5 min at room temperature, which prolonged lifetime and enhanced intensity of phosphorescence emissions. The conjugated planes were parallel to each other as evidenced by analysis of their single-crystal structures, which showed sequential stacking with a 0° dihedral angle (Fig. 10C). The electron cloud was driven from the benzothiazine dioxide to the phenyl group by the electron withdrawing group, and the electron density in the conjugation center increased, allowing for a more tightly overlapping π - π interaction. In addition, the n - π transition was induced by UV irradiation, which conformed to the electron flow trend, and the binding of energy levels was further enhanced, thereby stabilizing the triplet excited state for phosphorescence emission. However, the adhibition of these phosphorescence compounds in bioimaging was limited by the stringency of π - π

interactions in the solid crystals. To address this, a top-down approach was used to stabilize triplet excited states of RTP materials. Sonication of CS-F with F127 in aqueous solution resulted in nanoparticles that maintained the expected photophysical properties. Phosphorescence of CS-F nanoparticles was evaluated by intracutaneous injection into live mice (Fig. 10D). Strong phosphorescence signals were detected in the draining lymph nodes, indicative of nanoparticle accumulation. Fluorescence imaging did not show detectable signal, which again demonstrated that advantages of phosphorescence imaging adhibitions of pure organic mediums.

4.3. Aggregation-induced emission by RTP luminogens

Organic fluorescent probes can possess aggregation-induced emission (AIE) properties, which are valuable tools in biomedical applications due to their high photobleaching threshold, capacity to induce a large Stokes shift, and ability to activate fluorophore emission [103,104].

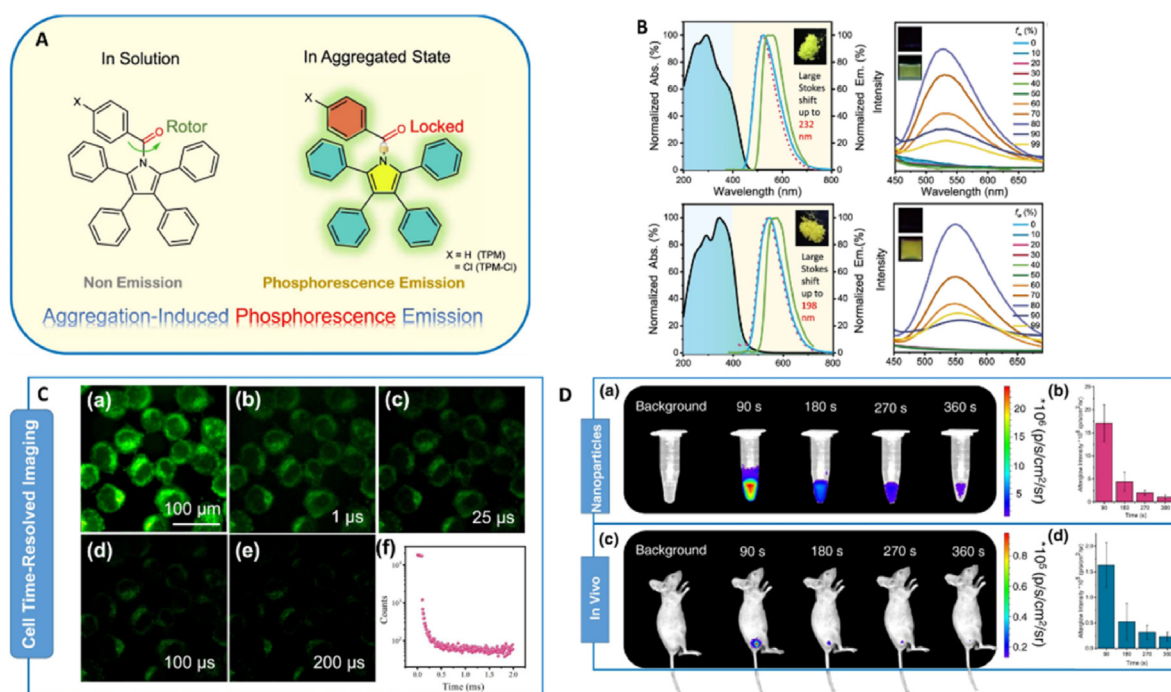


Fig. 12. (A) The molecular design strategy for the AIP compounds. (B) UV absorption spectra and phosphorescence spectra of TPM and TPM-Cl crystalline nanoparticles. (C) Images of HeLa cells at different time-points. (D) *In vivo* RTP imaging of the developed AIP following subcutaneous injection of TPM. [106].

Biocompatible AIE offer an attractive tool to realize image-guided surgery and the live monitoring of diverse biological processes. However, AIE have been limited by low SBR resulting from interference by tissue autofluorescence. Pure organic p-RTP materials can circumvent the interference of biological autofluorescence to provide a stable, high SBR luminescence signal. Furthermore, the single-state energy of the luminous material is higher than triple-state energy, which has a large Stokes displacement. Hence, integrating AIE and RTP characteristics into bioimaging materials could overcome the limitations of both to simultaneously take advantage of long-lasting imaging and high SBR, respectively.

Fabrication of organic RTP materials with considerably high efficiency and long lifetime remains a challenge due to the necessity for stabilized triplet excitons. In 2021, the Ding lab proposed a new idea to fine-tune molecular stacking through the modification of short alkyl chains to improve phosphorescence lifetime and phosphorescence quantum yield [105]. Through considered molecular design, they exploited a range of pure organic RTP materials (CBA). The introduction of short alkyl chains to RTP materials effectively improved their luminescence properties whilst in aggregated states due to molecular packing (Fig. 11A), and introduction of methyl groups (CBA-CH₃) demonstrated the further enhancement of molecular packing and the superior aggregation-induced emission (AIE) properties coupled with fluorescence brightness. Crystalline photophysical data showed that the phosphorescence efficiency and lifetime of CBA-CH₃ was significantly improved compared to unmethylated CBA (6.22 vs 4.38%, 868 vs 564 ms). Single-crystal X-ray diffraction analysis of the CBA compounds indicated that introduced alkyl groups enlarged twist angles and facilitated more intermolecular interactions, which was suggested to be the primary reasons for their longer lifetimes. To demonstrate the bioimaging potential of CBA-CH₃, it was loaded into amphiphilic co-polymer (MPEG2000-DSPE) micellar nanoparticles, which maintained strong RTP properties. Cytocompatibility and cell imaging were verified before the nanoparticles were systemically administered to live mice. The CBA-CH₃ nanoparticles showed a high SBR in both the lymph nodes and the in lung metastatic tumors (Fig. 11B). This work showed that molecular packing can be fine-tuned by adjusting the molecular side chain groups, to significantly improve the phosphorescence properties of RTP materials.

In 2021, the Zhang lab introduced aromatic carbonyl groups into tetraphenyl pyrrole molecules, creating two RTP compounds with AIE properties: phenyl-(2,3,4,5-tetraphenyl-1H-pyrrol-1-yl) methanone (TPM) and (4-chlorophenyl)-(2,3,4,5-tetraphenyl-1H-pyrrol-1-yl) methanone (TPM-Cl) (Fig. 12A) [106]. These molecules showed RTP emissions whilst in their agglomeration state, but not whilst dispersed in solution. This 'on-off switch' is an ideal characteristic of RTP materials for bioimaging. The team went on to prepare bright nanoparticles using a simplistic nanoprecipitation method (Fig. 12B), which resulted in TPM and TPM-Cl crystalline nanoparticles with a long emission lifetime (20 μs) capable of time-resolved imaging without background noise from cell autofluorescence (Fig. 12C) or tissue background noise (Fig. 12D). NIR light stimulated nanoparticles via two-photon absorption, which suggested broad application prospects in optical imaging of deep tissues with lower phototoxicity. The longevity, NIR emission, and low cytotoxicity properties of TPM suggest that these are promising organic aggregation-induced phosphorescence (AIP) materials for the development of theranostics, bioimaging, and imaging-guided surgery. The continued development and integration of AIP materials holds promise in the diversification and expansion of the bioimaging agent pool, which lend themselves to the promoted development of high-performance biological probes.

5. Conclusions

Organic persistent luminescence imaging techniques (CL, AL, RTP) have developed significantly over the past few years, offering routes

towards sustainable luminescence imaging characterized by minimal background noise, high SBR, deeper penetrability, and higher detection sensitivity than traditional fluorescence imaging. The elimination of the requirement of real time excitation, carcinogenic and inorganic components such as heavy metal ions, has resulted in high-performance and highly biocompatible bioimaging probes with promising applicability for *in vivo* imaging. However, despite the remarkable progress in the OPLM field, 4 major areas of improvement are required: (1) imaging detection sensitivity and penetration depth - as an example could be enhanced by further red-shift of emissions into the NIR-II spectra, which would also offer enhanced probe penetration depth; (2) the duration of OPLM fluorescence - it is necessary to improve the stability of OPLMs and develop probes that can output signals for a long time in the physiological and pathological tissue microenvironment; (3) development of cost-effective and simple scalable preparation strategies - the research in this area is still lacking; and (4) broadening applicability - current OPLM imaging research has mainly focused on cancer research, whereas wider applicability in other chronic or life-threatening diseases, such as autoimmune diseases, neurological diseases, and diabetes, have rarely been studied using OPLMs. It is foreseeable that the continued improvement of organic persistent luminescence probes will improve accuracy of bioimaging detection in deeper and smaller biological sites, whilst broadened application prospects will be achieved through integration of persistent luminescence probes into theranostic techniques for a diverse range of diseases. The concomitant development of persistent luminescence probes in these areas will not only contribute to more accurate clinical diagnosis and prognosis, but also provide enlightenment for the discovery of novel biological applicability and disease bioimaging.

Declaration of competing interest

The authors declare the following financial interests/personal relationships which may be considered as potential competing interests: Adam Midgley reports financial support was provided by National Natural Science Foundation of China. Deling Kong reports financial support was provided by National Natural Science Foundation of China. Dan Ding reports financial support was provided by National Key Research and Development Program of China Stem Cell and Translational Research.

Data availability

No data was used for the research described in the article.

Acknowledgments

This work was supported by the National Key R&D Program of China (Intergovernmental Cooperation Project, 2017YFE0132200) and National Natural Science Foundation of China (NSFC) projects (81921004, 81830060, 82050410449).

References

- [1] B.R. Smith, S.S. Gambhir, Nanomaterials for *in vivo* imaging, *Chem. Rev.* 117 (3) (2017) 901–986, <https://doi.org/10.1021/acs.chemrev.6b00073>.
- [2] B.C. Wilson, M. Jermyn, F. Leblond, Challenges and opportunities in clinical translation of biomedical optical spectroscopy and imaging, *J. Biomed. Opt.* 23 (3) (2018), 030901, <https://doi.org/10.1117/1.JBO.23.3.030901>.
- [3] P.F. Liu, X.Y. Mu, X.D. Zhang, et al., The Near-infrared-II fluorophores and advanced microscopy technologies development and application in bioimaging, *Bioconjugate Chem.* 31 (2) (2020) 260–275, <https://doi.org/10.1021/acs.bioconjchem.9b00610>.
- [4] A.J. Shuhendler, K.Y. Pu, L.N. Cui, et al., Real-time imaging of oxidative and nitrosative stress in the liver of live animals for drug-toxicity testing, *Nat. Biotechnol.* 32 (2014) 373–380, <https://doi.org/10.1038/nbt.2838>.
- [5] G.X. Feng, G.Q. Zhang, D. Ding, Design of superior phototheranostic agents guided by Jablonski diagrams, *Chem. Soc. Rev.* 49 (2020) 8179–8234, <https://doi.org/10.1039/D0CS00671H>.
- [6] W.B. Zhao, Y. Wang, K.K. Liu, R. Zhou, C.X. Shan, Multicolor biomass based carbon nanodots for bacterial imaging, *Chin. Chem. Lett.* 33 (2) (2022) 798–802, <https://doi.org/10.1016/j.ccl.2021.08.084>.

- [7] S.K. Sun, H.F. Wang, X.P. Yan, Engineering persistent luminescence nanoparticles for biological applications: from biosensing/bioimaging to theranostics, *Acc. Chem. Res.* 51 (5) (2018) 1131–1143, <https://doi.org/10.1021/acs.accounts.7b00619>.
- [8] J.H. Liu, T. Lécuyer, J. Seguin, et al., Imaging and therapeutic applications of persistent luminescence nanomaterials, *Adv. Drug Deliv. Rev.* 138 (1) (2019) 193–210, <https://doi.org/10.1016/j.addr.2018.10.015>.
- [9] Y.R. Tang, H.J. Song, Y.Y. Su, et al., Turn-on persistent luminescence probe based on graphitic carbon nitride for imaging detection of biothiols in biological fluids, *Anal. Chem.* 85 (24) (2013) 11876–11884, <https://doi.org/10.1021/ac403517u>.
- [10] Y. Li, M. Gecevicius, J.R. Qiu, Long persistent phosphors from fundamentals to applications, *Chem. Soc. Rev.* 45 (2016) 2090–2136, <https://doi.org/10.1039/C5CS00582E>.
- [11] J. Wang, Q.Q. Ma, Y.Q. Wang, et al., Recent progress in biomedical applications of persistent luminescence nanoparticles, *Nanoscale* 9 (2017) 6204–6218, <https://doi.org/10.1039/C7NR01488K>.
- [12] A. Harizaj, O.Q. De Clercq, B. Descamps, et al., Biocompatible lipid-coated persistent luminescent nanoparticles for in vivo imaging of dendritic cell migration, *Part. Part. Syst. Charact.* 36 (11) (2019), 1900371, <https://doi.org/10.1002/ppsc.201900371>.
- [13] H.X. Zhao, C.X. Yang, X.P. Yan, Fabrication and bioconjugation of biii and criii Co-doped ZnGa₂O₄ persistent luminescent nanoparticles for dual-targeted cancer bioimaging, *Nanoscale* 8 (2016), 18987–18994, <https://doi.org/10.1039/C6NR06259H>.
- [14] H.X. Tan, T.Y. Wang, Y.R. Shao, et al., Crucial breakthrough of functional persistent luminescence materials for biomedical and information technological applications, *Front. Chem.* 7 (2019) 387, <https://doi.org/10.3389/fchem.2019.00387>.
- [15] Q.S. Lin, Z.H. Li, Q. Yuan, Recent advances in autofluorescence-free biosensing and bioimaging based on persistent luminescence nanoparticles, *Chin. Chem. Lett.* 30 (9) (2019) 1547–1556, <https://doi.org/10.1016/j.ccl.2019.06.016>.
- [16] R. Kabe, C. Adachi, Organic long persistent luminescence, *Nature* 550 (2017) 384–387, <https://doi.org/10.1038/nature24010>.
- [17] K. Li, T.B. Ren, S.Y. Huan, et al., Progress and perspective of solid-state organic fluorophores for biomedical applications, *J. Am. Chem. Soc.* 143 (50) (2021) 21143–21160, <https://doi.org/10.1021/jacs.1c10925>.
- [18] A.S. Klymchenko, Solvatochromic and fluorogenic dyes as environment-sensitive probes: design and biological applications, *Acc. Chem. Res.* 50 (2) (2017) 366–375, <https://doi.org/10.1021/acs.accounts.6b00517>.
- [19] H.B. Cheng, Y.Y. Li, B.Z. Tang, J.Y. Yoon, Assembly strategies of organic-based imaging agents for fluorescence and photoacoustic bioimaging applications, *Chem. Soc. Rev.* 49 (1) (2020) 21–31, <https://doi.org/10.1039/C9CS00326F>.
- [20] Y. Li, Y.F. Liu, Q.Q. Li, et al., Novel NIR-II organic fluorophores for bioimaging beyond 1550 nm, *Chem. Sci.* 11 (10) (2020) 2621–2626, <https://doi.org/10.1039/C9SC06567A>.
- [21] L. Liang, N. Chen, Y.Y. Jia, et al., Recent progress in engineering near-infrared persistent luminescence nanoprobes for time-resolved biosensing/bioimaging, *Nano Res.* 12 (2019) 1279–1292, <https://doi.org/10.1007/s12274-019-2343-6>.
- [22] C. Dodeigne, L. Thunus, R. Lejeune, Chemiluminescence as diagnostic tool. A review, *Talanta* 51 (3) (2000) 415–439, [https://doi.org/10.1016/S0039-9140\(99\)00294-5](https://doi.org/10.1016/S0039-9140(99)00294-5).
- [23] Y.Y. Jiang, K.Y. Pu, Molecular probes for autofluorescence-free optical imaging, *Chem. Rev.* 121 (21) (2021) 13086–13131, <https://doi.org/10.1021/acs.chemrev.1c00506>.
- [24] Y.L. Yang, F. Zhang, Activatable chemiluminescent molecular probes for bioimaging and biosensing, *Anal. Sens.* 1 (2) (2021) 75–89, <https://doi.org/10.1002/ansc.202000033>.
- [25] M.A. Tzani, D.K. Gioxidis, M.G. Kallitsakis, Direct and indirect chemiluminescence: reactions, mechanisms and challenges, *Molecules* 26 (24) (2021), <https://doi.org/10.3390/molecules26247664>.
- [26] J.H. Zhi, Q. Zhou, H.F. Shi, et al., Organic room temperature phosphorescence materials for biomedical applications, *Chem. Asian J.* 15 (7) (2020) 947–957, <https://doi.org/10.1002/asia.201901658>.
- [27] M.W. Yang, J.G. Huang, J.L. Fan, J.J. Du, K.Y. Pu, X.J. Peng, Chemiluminescence for bioimaging and therapeutics: recent advances and challenges, *Chem. Soc. Rev.* 49 (2020) 6800–6815, <https://doi.org/10.1039/D0CS00348D>.
- [28] A.M. García-Campaña, W.R.G. Baeyens, Principles and recent analytical applications of chemiluminescence, *Analisis* 28 (8) (2000) 686–698, <https://doi.org/10.1051/analisis:2000280686>.
- [29] K. Suzuki, T. Nagai, Recent progress in expanding the chemiluminescent toolbox for bioimaging, *Curr. Opin. Biotechnol.* 48 (2017) 135–141, <https://doi.org/10.1016/j.copbio.2017.04.001>.
- [30] E.H. White, F. McCapra, G.F. Field, W.D. McElroy, The structure and synthesis of firefly luciferin, *J. Am. Chem. Soc.* 83 (1961) 2402–2403, <https://doi.org/10.1021/ja00886a019>.
- [31] T. Goto, T. Takagi, Chemiluminescence of a Cypridina luciferin analogue, 2-methyl-6-phenyl-3,7-dihydroimidazo[1,2-a]pyrazin-3-One, in the presence of the xanthine-xanthine oxidase system, *BCSJ* 53 (3) (1980) 833–834, <https://doi.org/10.1246/bcsj.53.833>.
- [32] S. Yagur-Kroll, B. Bilic, S. Belkin, Strategies for enhancing bioluminescent bacterial sensor performance by promoter region manipulation: enhancing bacterial sensor performance, *Microb. Biotechnol.* 3 (3) (2010) 300–310, <https://doi.org/10.1111/j.1751-7915.2009.00149.x>.
- [33] S. Gnaim, D. Shabat, Activity-based optical sensing enabled by self-immolative scaffolds: monitoring of release events by fluorescence or chemiluminescence output, *Acc. Chem. Res.* 52 (10) (2019) 2806–2817, <https://doi.org/10.1021/acs.accounts.9b00338>.
- [34] U. Haris, H.N. Kagalwala, Y.L. Kim, A.R. Lippert, Seeking illumination: the path to chemiluminescent 1,2-dioxetanes for quantitative measurements and in vivo imaging, *Acc. Chem. Res.* 54 (13) (2021) 2844–2857, <https://doi.org/10.1021/acs.accounts.1c00185>.
- [35] N. Hananya, D. Shabat, Recent advances and challenges in luminescent imaging: bright outlook for chemiluminescence of dioxetanes in water, *ACS Cent. Sci.* 5 (6) (2019) 949–959, <https://doi.org/10.1021/acscentsci.9b00372>.
- [36] Y.J. Wang, L.N. Shi, Z.F. Ye, et al., Reactive oxygen correlated chemiluminescent imaging of a semiconducting polymer nanoplatfor for monitoring chemodynamic therapy, *Nano Lett.* 20 (1) (2020) 176–183, <https://doi.org/10.1021/acs.nanolett.9b03556>.
- [37] L.F.M.L. Ciscato, F.H. Bartoloni, D. Weiss, et al., Experimental evidence of the occurrence of intramolecular electron transfer in catalyzed 1, 2-dioxetane decomposition, *J. Org. Chem.* 75 (19) (2010) 6574–6580, <https://doi.org/10.1021/jo1013405>.
- [38] D. Wu, J.J. Zhou, M.N. Creyer, et al., Phenolic-enabled nanotechnology: versatile particle engineering for biomedicine, *Chem. Soc. Rev.* 50 (2021) 4432–4483, <https://doi.org/10.1039/D0CS00908C>.
- [39] N. Hananya, D. Shabat, A Glowing trajectory between bio- and chemiluminescence: from luciferin-based probes to triggerable dioxetanes[J], *Angew. Chem., Int. Ed.* 56 (52) (2017) 16454–16463, <https://doi.org/10.1002/anie.201706969>.
- [40] M.W. Yang, J.G. Huang, J.L. Fan, et al., Chemiluminescence for bioimaging and therapeutics: recent advances and challenges, *Chem. Soc. Rev.* 49 (19) (2020) 6800–6815, <https://doi.org/10.1039/D0CS00348D>.
- [41] S. Gnaim, O. Green, D. Shabat, The emergence of aqueous chemiluminescence: new promising class of phenoxy 1,2-dioxetane luminophores, *Chem. Commun.* 54 (17) (2018) 2073–2085, <https://doi.org/10.1039/C8CC00428E>.
- [42] H.O. Albrecht, Über die Chemiluminescenz des Aminophthalsäurehydrazids" (On the chemiluminescence of aminophthalic acid hydrazide), *Zeitschrift für Physikalische Chemie. Z. Phys. Chem.* 136 (1928) 321–330, <https://doi.org/10.1515/zpch-1928-13625>.
- [43] X.Q. Xu, H.J. An, D.L. Zhang, et al., A self-illuminating nanoparticle for inflammation imaging and cancer therapy, *Sci. Adv.* 5 (1) (2019), <https://doi.org/10.1126/sciadv.aat2953>, 2019.
- [44] O. Green, S. Gnaim, R. Blau, A. Eldar-Boock, R. Satchi-Fainaru, D. Shabat, Near-infrared dioxetane luminophores with direct chemiluminescence emission mode, *J. Am. Chem. Soc.* 139 (37) (2017) 13243–13248, <https://doi.org/10.1021/jacs.7b08446>.
- [45] R. Radi, T.P. Cosgrove, J.S. Beckman, et al., Peroxynitrite-induced luminol chemiluminescence[J], *Biochem. J.* 290 (1) (1993) 51–57, <https://doi.org/10.1042/bj2900051>.
- [46] E.S. Lee, V.G. Deepagan, D.G. You, et al., Nanoparticles based on quantum dots and a luminol derivative: implications for in vivo imaging of hydrogen peroxide by chemiluminescence resonance energy transfer, *Chem. Commun.* 52 (22) (2016) 4132–4135, <https://doi.org/10.1039/C5CC09850E>.
- [47] O. Shimomura, T. Goto, Y. Hirata, Crystalline Cypridina luciferin, *Bull. Chem. Soc. Jpn.* 30 (1957) 929–933, <https://doi.org/10.1246/bcsj.30.929>.
- [48] J. Sousa, C.M. Magalhães, P. González-Berduelas, et al., Comparative investigation of the chemiluminescent properties of a dibrominated coelenterazine analog, *Int. J. Mol. Sci.* 23 (15) (2022) 8490, <https://doi.org/10.3390/ijms23158490>.
- [49] P. Li, L. Liu, H.B. Xiao, W. Zhang, L.L. Wang, B. Tang, A new polymer nanoprobe based on chemiluminescence resonance energy transfer for ultrasensitive imaging of intrinsic superoxide anion in mice, *J. Am. Chem. Soc.* 138 (9) (2016) 2893–2896, <https://doi.org/10.1021/jacs.5b11784>.
- [50] A.P. Schaap, S.D. Gagnon, Chemiluminescence from a phenoxide-substituted 1, 2-dioxetane: a model for firefly bioluminescence[J], *J. Am. Chem. Soc.* 104 (12) (1982) 3504–3506, <https://doi.org/10.1021/ja00376a044>.
- [51] S. Ye, N. Hananya, O. Green, et al., A highly selective and sensitive chemiluminescent probe for real-time monitoring of hydrogen peroxide in cells and animals, *Angew. Chem., Int. Ed.* 59 (34) (2020) 14326–14330, <https://doi.org/10.1002/anie.202005429>.
- [52] D. Cui, J.C. Li, X.H. Zhao, K.Y. Pu, R.P. Zhang, Semiconducting polymer nanoparticles for near-infrared chemiluminescence imaging of immunoactivation, *Adv. Mater.* 32 (6) (2020), 1906314, <https://doi.org/10.1002/adma.201906314>.
- [53] J.G. Huang, Y. Lyu, J.C. Li, et al., A renal-clearable duplex optical reporter for real-time imaging of contrast-induced acute kidney injury, *Angew. Chem., Int. Ed.* 58 (49) (2019) 17796–17804, <https://doi.org/10.1002/ange.201910137>.
- [54] M. Di Fusco, A. Quintavalla, C. Trombini, et al., Preparation and characterization of the thermochemiluminescent acridine-containing 1, 2-dioxetanes as promising ultrasensitive labels in bioanalysis[J], *J. Org. Chem.* 78 (22) (2013) 11238–11246, <https://doi.org/10.1021/jo401683r>.
- [55] X. Ni, X.Y. Zhang, X.C. Duan, H.L. Zheng, X.S. Xue, D. Ding, Near-infrared afterglow luminescent aggregation-induced emission dots with ultrahigh tumor-to-liver signal ratio for promoted image-guided cancer surgery, *Nano Lett.* 19 (1) (2019) 318–330, <https://doi.org/10.1021/acs.nanolett.8b03936>.
- [56] C. Chen, H.Q. Gao, H.L. Ou, R.T.K. Kwok, Y.H. Tang, D.H. Zheng, D. Ding, Amplification of activated near-infrared afterglow luminescence by introducing twisted molecular geometry for understanding neutrophil-involved diseases, *J. Am. Chem. Soc.* 144 (8) (2022) 3429–3441, <https://doi.org/10.1021/jacs.1c11455>.
- [57] J.Y. Liu, Z.X. Chen, H.Q. Huo, L.L. Chen, Y. Wu, X. Zhang, L.C. Su, Q. Li, J.B. Song, An activatable near-infrared molecular chemiluminescence probe for visualization

- of NQO1 activity in vivo, *Chin. J. Chem.* 40 (20) (2022) 2400–2406, <https://doi.org/10.1002/cjoc.202200300>.
- [58] S. Ye, B.W. Yang, M.L. Wu, Z.F. Chen, J.G. Shen, D. Shabat, D. Yang, Recurring real-time monitoring of inflammations in living mice with a chemiluminescent probe for hypochlorous acid, *CCS Chem.* 4 (6) (2022) 1871–1878, <https://doi.org/10.31635/ccschem.021.202101108>.
- [59] M.S.C. Peukert, S.P. Gholap, O. Green, L. Pinkert, J. Heuvel, M. Ham, D. Shabat, M. Brönstrup, Enzyme-activated, chemiluminescent siderophore-dioxetane probes enable the selective and highly sensitive detection of bacterial pathogens, *Angew. Chem., Int. Ed.* 61 (25) (2022), <https://doi.org/10.1002/anie.202201423> e202201423.
- [60] L. Delafresnaye, F.R. Bloesser, K.B. Kockler, C.W. Schmitt, I.M. Irshadeen, C. Barner-Kowollik, All eyes on visible-light peroxyoxalate chemiluminescence read-out systems, *Chem.–Eur. J.* 26 (1) (2020) 114–127, <https://doi.org/10.1002/chem.201904054>.
- [61] S.A. Tonkin, R. Bos, G.A. Dyson, et al., Studies on the mechanism of the peroxyoxalate chemiluminescence reaction, *Anal. Chim. Acta* 614 (2) (2008) 173–181, <https://doi.org/10.1016/j.ata.2008.03.009>.
- [62] P. Farahani, W.J. Baader, Unimolecular decomposition mechanism of 1,2-dioxetanedione: concerted or biradical? That is the question, *J. Phys. Chem. A* 121 (6) (2017) 1189–1194, <https://doi.org/10.1021/acs.jpca.6b10365>.
- [63] G.A. Souza, A.P. Lang, W.J. Baader, Mechanistic studies on the peroxyoxalate chemiluminescence using sodium salicylate as base catalyst, *Photochem. Photobiol.* 93 (6) (2017) 1423–1429, <https://doi.org/10.1111/php.12797>.
- [64] Y.L. Yang, S.F. Wang, L.F. Lu, Q.S. Zhang, P. Yu, Y. Fan, F. Zhang, NIR-II chemiluminescence molecular sensor for in vivo high-contrast inflammation imaging, *Angew. Chem., Int. Ed.* 59 (42) (2020) 18380–18385, <https://doi.org/10.1002/ange.202007649>.
- [65] Y. Yu, B.R. Xie, X.H. Liu, J.J. Ye, H. Cheng, Z.L. Zhong, X.Z. Zhang, A H2O2-responsive theranostic platform for chemiluminescence detection and synergistic therapy of tumors, *J. Mater. Chem. B* 10 (2022) 1634–1640, <https://doi.org/10.1039/D2TB00015F>.
- [66] S. Xu, R.F. Chen, C. Zheng, W. Huang, Excited state modulation for organic afterglow: materials and applications, *Adv. Mater.* 28 (45) (2016) 9920–9940, <https://doi.org/10.1002/adma.201602604>.
- [67] S. Xu, W. Wang, H. Li, et al., Design of highly efficient deep-blue organic afterglow through guest sensitization and matrices rigidification, *Nat. Commun.* (2020) 4802, <https://doi.org/10.1038/s41467-020-18572-9>.
- [68] Y. Lyu, D. Cui, J.G. Huang, W.X. Fan, Y.S. Miao, K.Y. Pu, Near-infrared afterglow semiconducting nano-polycomplexes for the multiplex differentiation of cancer exosomes, *Angew. Chem., Int. Ed.* 131 (15) (2019) 5037–5041, <https://doi.org/10.1002/ange.201900092>.
- [69] X. Zhen, C. Xie, K.Y. Pu, Temperature-correlated afterglow of a semiconducting polymer nanococktail for imaging-guided photo-thermal therapy, *Angew. Chem., Int. Ed.* 130 (15) (2018) 4002–4006, <https://doi.org/10.1002/ange.201712550>.
- [70] O.P. Dimitriev, Dynamics of excitons in conjugated molecules and organic semiconductor systems, *Chem. Rev.* 122 (9) (2022) 8487–8593, <https://doi.org/10.1021/acs.chemrev.1c00648>.
- [71] X.C. Duan, G.Q. Zhang, S.L. Ji, Y.M. Zhang, J. Li, H.L. Ou, Z.Y. Gao, G.X. Feng, D. Ding, Activatable persistent luminescence from porphyrin derivatives and supramolecular probes with imaging-modality transformable characteristics for improved biological applications, *Angew. Chem., Int. Ed.* 61 (24) (2022), e202116174, <https://doi.org/10.1002/anie.202116174>.
- [72] W. Chen, Y. Zhang, Q. Li, et al., Near-infrared afterglow luminescence of chlorin nanoparticles for ultrasensitive in vivo imaging, *J. Am. Chem. Soc.* 144 (15) (2022) 6719–6726, <https://doi.org/10.1021/jacs.1c10168>.
- [73] X.P. Wang, Y. Sun, G.M. Wang, J.Y. Li, K.K. Zhang, TADF-type organic afterglow, *Angew. Chem., Int. Ed.* 60 (31) (2021) 17138–17147, <https://doi.org/10.1002/anie.202105628>.
- [74] J. Wang, J.L. Li, J.N. Yu, H.W. Zhang, B.B. Zhang, Large hollow cavity luminous nanoparticles with near-infrared persistent luminescence and tunable sizes for tumor afterglow imaging and chemo-photodynamic therapies, *ACS Nano* 12 (5) (2018) 4246–4258, <https://doi.org/10.1021/acsnano.7b07606>.
- [75] Q.Q. Miao, C. Xie, X. Zhen, Y. Lyu, H.W. Duan, X.G. Liu, J.V. Jokerst, K.Y. Pu, Molecular afterglow imaging with bright, biodegradable polymer nanoparticles, *Nat. Biotechnol.* 35 (2017) 1102–1110, <https://doi.org/10.1038/nbt.3987>.
- [76] D. Cui, C. Xie, J.C. Li, Y. Lyu, K.Y. Pu, Semiconducting photosensitizer-incorporated copolymers as near-infrared afterglow nanoagents for tumor imaging, *Adv. Healthcare Mater.* 7 (18) (2018) 1800329, <https://doi.org/10.1002/adhm.201800329>.
- [77] C. Xie, X. Zhen, Q.Q. Miao, Y. Lyu, K.Y. Pu, Self-assembled semiconducting polymer nanoparticles for ultrasensitive near-infrared afterglow imaging of metastatic tumors, *Adv. Mater.* 30 (21) (2018), e1801331, <https://doi.org/10.1002/adma.201801331>.
- [78] Y.Y. Jiang, J.G. Huang, X. Zhen, et al., A generic approach towards afterglow luminescent nanoparticles for ultrasensitive in vivo imaging, *Nat. Commun.* 2064 (10) (2019), <https://doi.org/10.1038/s41467-019-10119-x>.
- [79] S.S. He, C. Xie, Y. Jiang, et al., An organic afterglow protheranostic nanoassembly, *Adv. Mater.* 31 (32) (2019), 1902672, <https://doi.org/10.1002/adma.201902672>.
- [80] C.G. Qian, J.C. Yu, Y.L. Chen, et al., Light-activated hypoxia-responsive nanocarriers for enhanced anticancer therapy, *Adv. Mater.* 28 (17) (2016) 3313–3320, <https://doi.org/10.1002/adma.201505869>.
- [81] K.Y. Pu, A.J. Shuhendler, J.V. Jokerst, et al., Semiconducting polymer nanoparticles as photoacoustic molecular imaging probes in living mice, *Nat. Nanotechnol.* 9 (2014) 233–239, <https://doi.org/10.1038/nnano.2013.302>.
- [82] G.S. Hong, Y.P. Zou, A.L. Antaris, et al., Ultrafast fluorescence imaging in vivo with conjugated polymer fluorophores in the second near-infrared window, *Nat. Commun.* 4206 (5) (2014), <https://doi.org/10.1038/ncomms5206>.
- [83] Q. Zhao, F.Y. Li, C.H. Huang, Phosphorescent chemosensors based on heavy-metal complexes [J], *Chem. Soc. Rev.* 39 (8) (2010) 3007–3030, <https://doi.org/10.1039/B915340C>.
- [84] Q. Wu, H. Ma, K. Ling, et al., Reversible ultralong organic phosphorescence for visual and selective chloroform detection [J], *ACS Appl. Mater. Interfaces* 10 (39) (2018) 33730–33736, <https://doi.org/10.1021/acsaami.8b13713>.
- [85] Y. Yang, K.Z. Wang, D. Yan, Ultralong persistent room temperature phosphorescence of metal coordination polymers exhibiting reversible pH-responsive emission, *ACS Appl. Mater. Interfaces* 8 (24) (2016) 15489–15496, <https://doi.org/10.1021/acsami.6b03956>.
- [86] G.Q. Zhang, G.M. Palmer, M.W. Dewhurst, et al., A dual-emissive-materials design concept enables tumour hypoxia imaging [J], *Nat. Mater.* 8 (9) (2009) 747–751, <https://doi.org/10.1038/nmat2509>.
- [87] Y.T. Tao, Q. Wang, C.L. Yang, et al., A simple carbazole/oxadiazole hybrid molecule: an excellent bipolar host for green and red phosphorescent OLEDs, *Angew. Chem., Int. Ed.* 47 (42) (2008) 8104–8107, <https://doi.org/10.1002/anie.200803396>.
- [88] L. Gu, H.F. Shi, L.F. Bian, et al., Colour-tunable ultra-long organic phosphorescence of a single-component molecular crystal, *Nat. Photonics* 13 (6) (2019) 406–411, <https://doi.org/10.1038/s41566-019-0408-4>.
- [89] Z.H. He, H.Q. Gao, S.T. Zhang, et al., Achieving persistent, efficient, and robust room-temperature phosphorescence from pure organics for versatile applications, *Adv. Mater.* 31 (18) (2019), e1807222, <https://doi.org/10.1002/adma.201807222>.
- [90] Y.J. Xie, Y.W. Ge, Q. Peng, et al., How the molecular packing affects the room temperature phosphorescence in pure organic compounds: ingenious molecular design, detailed crystal analysis, and rational theoretical calculations, *Adv. Mater.* 29 (17) (2017), 1606829, <https://doi.org/10.1002/adma.201606829>.
- [91] Y.Q. You, K.W. Huang, X.J. Liu, et al., Hydrophilic ultralong organic nanophosphors, *Small* 16 (8) (2020), 1906733, <https://doi.org/10.1002/sml.201906733>.
- [92] P.C. Xue, J.B. Sun, P. Chen, et al., Luminescence switching of a persistent room-temperature phosphorescent pure organic molecule in response to external stimuli, *Chem. Commun.* 51 (52) (2015) 10381–10384, <https://doi.org/10.1039/C5CC03403E>.
- [93] Y. Xiong, Z. Zhao, W.J. Zhao, et al., Designing efficient and ultralong pure organic room-temperature phosphorescent materials by structural isomerism, *Angew. Chem., Int. Ed.* 57 (27) (2018) 7997–8001, <https://doi.org/10.1002/ange.201800834>.
- [94] X.K. Ma, Y. Liu, Supramolecular purely organic room-temperature phosphorescence, *Acc. Chem. Res.* 54 (17) (2021) 3403–3414, <https://doi.org/10.1021/acs.accounts.1c00336>.
- [95] W.J. Zhao, Z.K. He, Q. Peng, et al., Highly sensitive switching of solid-state luminescence by controlling intersystem crossing, *Nat. Commun.* 3044 (9) (2018), <https://doi.org/10.1038/s41467-018-05476-y>.
- [96] Q.X. Dang, Y.Y. Jiang, J.F. Wang, et al., Room-temperature phosphorescence resonance energy transfer for construction of near-infrared afterglow imaging agents, *Adv. Mater.* 32 (52) (2020), 2006752, <https://doi.org/10.1002/adma.202006752>.
- [97] O. Bolton, K. Lee, H.J. Kim, et al., Activating efficient phosphorescence from purely organic materials by crystal design, *Nat. Chem.* 3 (3) (2011) 205, <https://doi.org/10.1038/nchem.984>.
- [98] K. Jinnai, R. Kabe, Z. Lin, C. Adachi, Organic long-persistent luminescence stimulated by visible light in p-type systems based on organic photoredox catalyst dopants, *Nat. Mater.* 21 (2022) 338–344, <https://doi.org/10.1038/s41563-021-01150-9>.
- [99] T.T. Zhang, H.Q. Gao, A.Q. Lv, et al., Hydrogen bonding boosted the persistent room temperature phosphorescence of pure organic compounds for multiple applications, *J. Mater. Chem. C* 7 (29) (2019) 9095–9101, <https://doi.org/10.1039/C9TC02879J>.
- [100] Y.Y. Fan, S.W. Liu, M. Wu, et al., Mobile phone flashlight-excited red afterglow bioimaging, *Adv. Mater.* 34 (18) (2022), e2201280, <https://doi.org/10.1002/adma.202201280>.
- [101] X. Zhen, Y. Tao, Z.F. An, et al., Ultralong phosphorescence of water-soluble organic nanoparticles for in vivo afterglow imaging, *Adv. Mater.* 29 (33) (2017), <https://doi.org/10.1002/adma.201606665>.
- [102] J. Yang, X. Zhen, B. Wang, et al., The influence of the molecular packing on the room temperature phosphorescence of purely organic luminogens, *Nat. Commun.* 9 (1) (2018) 840, <https://doi.org/10.1038/s41467-018-03236-6>.
- [103] D. Ding, K. Li, B. Liu, B.Z. Tang, Bioprobes based on AIE fluorogens, *Acc. Chem. Res.* 46 (11) (2013) 2441–2453, <https://doi.org/10.1021/ar3003464>.
- [104] S.R. Jia, Z.Y. Gao, Z.L. Wu, H.Q. Gao, H. Wang, H.L. Ou, D. Ding, Sonosensitized aggregation-induced emission dots with capacities of immunogenic cell death induction and multivalent blocking of programmed cell death-ligand 1 for amplified antitumor immunotherapy, *CCS Chem.* 4 (2) (2021) 501–514, <https://doi.org/10.31635/ccschem.021.202101458>.
- [105] H.Q. Gao, Z.Y. Gao, D. Jiao, et al., Boosting room temperature phosphorescence performance by alkyl modification for intravital orthotopic lung tumor imaging, *Small* 17 (22) (2021), e2005449, <https://doi.org/10.1002/sml.202005449>.
- [106] J.H. Yang, Y.H. Zhang, X.H. Wu, et al., Rational design of pyrrole derivatives with aggregation-induced phosphorescence characteristics for time-resolved and two-photon luminescence imaging, *Nat. Commun.* 12 (1) (2021) 4883, <https://doi.org/10.1038/s41467-021-25174-6>.